ChemCatChem

Review
doi.org/10.1002/cctc.202201542

Chemistry Europe
European Chemical Societies Publishing

www.chemcatchem.org

Organophotocatalytic Mechanisms: Simplicity or Naïvety? Diverting Reactive Pathways by Modifications of Catalyst Structure, Redox States and Substrate Preassemblies

Mark John P. Mandigma,[a, b] Jaspreet Kaur,[a] and Joshua P. Barham*[a]

Dedicated to Professor Shigeru Yamago on the occasion of his 60th birthday.

Photocatalysis is a powerful tool to assemble diverse chemical scaffolds, yet a bottleneck on its further development is the understanding of the multitude of possible pathways when practitioners rely only on oversimplified thermodynamic and optical factors. Recently, there is a growing number of studies in the field that exploit, *inter alia*, kinetic parameters and organophotocatalysts that are synthetically more programmable in terms of their redox states and opportunities for aggregation with a target substrate. Non-covalent interactions play a key role that enables access to a new generation of reactivities such as those of open-shell organophotocatalysts. In this review, we discuss how targeted structural and redox modifications influence the organophotocatalytic mechanisms together with their underlying principles. We also highlight the benefits of strategies such as preassembly and static quenching that overcome common reactivity issues (e.g., diffusion rate limits and energetic limits).

1. Introduction

Arguably, the use of light to induce chemical reactions is one of the fastest growing and most powerful contemporary techniques in chemical research and manufacturing. In fact, the photon was acknowledged as a '21st century reagent.'[1] Although the term 'photocatalysis' (a process involving the use of a photon-absorbing species as a catalyst – a photocatalyst '**PC**') was coined as early as 1911,[2] only recently has the field enjoyed a period of renaissance as seen by an influx of studies over the last decade.[3] To put it in one statement, the enabling applications of photocatalysis are underpinned by accessing radical or 'open-shell' intermediates under exceedingly mild conditions, to rapidly build molecular complexity in a way that is often elusive for other reaction classes (i.e. ionic reactions or transition metal-catalyzed cross couplings).[4] While the use of transition metal polypyridyl complexes – such as those of [Ir] and [Ru] – jumpstarted the field,[5] a growing interest in cheaper, more sustainable, and more architecturally-tunable (i.e. in terms of synthetic modifications) alternatives has paved the way for the development of organic based **PC**s (hence the term organophotocatalysts, Org**PC**s).[6–12]

1.1. Basic mechanistic manifolds of (organo)photocatalysis

Given the rising importance of organophotocatalysis, it is important for an increasing number of practitioners to gain a deeper understanding in this field. Generally speaking, photocatalysis has three mechanistic paradigms (Figure 1A). In the crudest sense, consider the case when a closed-shell photocatalyst **PC** absorbs light: an electron (usually – but not necessarily – in the highest occupied molecular orbital, HOMO) is promoted to an unoccupied orbital (i.e. the lowest unoccupied molecular orbital, LUMO or LUMO + n, where n = an unoccupied molecular orbital with higher energies than the lowest one, following Laporte and spin selection rules). This essentially generates a photoexcited, 'diradical' species: ***PC**. By inspection of the singly-occupied molecular orbitals (SOMO) of ***PC** *versus* the HOMO and LUMO of **PC**, the first two mechanistic paradigms of the excited state become obvious: ***PC** can be an oxidant (due to its higher electron affinity, i.e. E_{ea} (***PC**) > E_{ea} (**PC**)) or a reductant (due to its lower ionization energy, E_i (***PC**) < E_i (**PC**)) for single electron transfer (SET) reactions. Together, these two mechanistic paradigms constitute a subset of photocatalysis called photoredox catalysis (PRC). The third mechanistic paradigm is through energy transfer (EnT) where there is no net movement of electrons between ***PC** and the substrate but an exchange of multiplicities. There are two modes by which EnT could happen. First is through Förster resonance energy transfer (FRET),[13] where the photoexcited donor **D*** excites the ground state acceptor **A** by coulombic interactions. However, a second mode of EnT is more appropriate in describing reactions in solution (i.e. majority of laboratory synthetic photocatalysis) and this is through Dexter energy transfer[14] where **D*** excites an acceptor molecule **A** through an intermolecular exchange of ground state and excited state electrons.[15]

1.2. (Organo)photocatalytic mechanisms are more than just thermodynamics and optics

Traditionally, until very recently, practitioners of synthetic photocatalysis heavily fixated on two dogmas when planning reactions or rationalizing results: i) thermodynamic feasibility of SET or EnT events (i.e. redox potentials of the excited photocatalyst and ground state target substrate) and ii) optical properties or excitation energies (i.e. λ_{max} in the UV-vis spectrum, singlet / triplet energies).[16,17] While these dogmas are of course fundamentally reasonable and they alone can suffice to explain reactive outcomes in many cases, practitioners who rely on such considerations alone are oftentimes naïve to the whole picture. As a result, a number of reaction conditions are determined empirically or serendipitously without realizing how or why the results occurred. Kinetic parameters should always be included as a consideration for both predicting and explaining reaction outcomes and we note the growing calls for such practice.[16,17] After all the term 'photocatalysis' bears the

[a] *M. J. P. Mandigma, J. Kaur, Dr. J. P. Barham*
Universität Regensburg
Fakultät für Chemie und Pharmazie
93040 Regensburg (Germany)
E-mail: Joshua-Philip.Barham@chemie.uni-regensburg.de
[b] *M. J. P. Mandigma*
University of Bristol
School of Chemistry
BS8 1TS Bristol (United Kingdom)

Supporting information for this article is available on the WWW under https://doi.org/10.1002/cctc.202201542

term 'catalysis' which is a substance that changes the rate (a keyword for kinetics)[18] of a reaction. One does not need a fully comprehensive description of all the physical chemistry and mathematics behind it, but to take in to account the key points and the practical aspects of the theories governing photochemical reaction rates (Figure 1A, right). For instance, SET – whether photoinduced or not – is governed by Marcus theory which states that the activation energy of SET ($\Delta G^{\neq}_{SET}$) depends not only on the free energy of SET (ΔG_{SET}) but also on the structural rigidity of reacting species (related to the internal reorganization energy, λ_i), the nature (i.e. polarity or dielectric constants) of solvent medium, and the molecular sizes of, or distance between reacting species (the latter two affecting the external reorganization energy λ_o). The square (parabolic nature) relationship between the ΔG_{SET} term and $\Delta G^{\neq}_{SET}$ signifies the presence of the Marcus inverted region. Practically speaking, this means that at a certain point when SET is too exergonic, the rate of electron transfer becomes slower and other mechanisms may take over. On the other hand, Dexter's theory of energy transfer relates the rate of EnT (as described by the rate constant k_{EnT}) with steric repulsions (related to an experimental factor K), excited triplet energies (where their difference estimates the efficiency of EnT as defined by the 'spectral overlap' term J)[19] and distance between donor **D** and acceptor **A** species (**D**-**A** or **PC**-substrate given by $-2R_{DA}$ /L term, where R_{DA} = distance between donor (**D**) and acceptor (**A**) which could be influenced by attractive non-covalent interactions, L = sum of their respective van der Waals radii). Aside from this, there are also many reactions occurring at an excitation wavelength (λ_{ex}) that is not the λ_{max} of a given absorption in the UV-visible spectra, and may even instead be a tailing feature. Oftentimes, this is due to non-covalent assemblies with the substrate (EDA complexes, or radical ion substrate assemblies) that absorb differently to the Org**PC** on its own.

1.3. Key strategies for catalyst modification that influence or divert photocatalytic mechanism

Another aspect to bear in mind is that the three mechanistic paradigms are *often not exclusive* – that means competing multiple pathways could operate in one system. Knowledge of how these pathways interplay – through the thermodynamic, optical, as well as kinetic lenses outlined above – could actually

Mark John P. Mandigma was born in Negros Occidental, Philippines. He received his B.Sc. degree from University of Santo Tomas (Philippines) under the supervision of Prof. Allan Patrick G. Macabeo in 2017. He received his M.Sc. degree from the Elite Network of Bavaria's Synthesis and Catalysis (SynCat) Master program in 2022, under the supervision of Dr. Joshua P. Barham at the University of Regensburg (Germany). His research in the Barham group involved i) organophotocatalysis under gas-liquid flow conditions, ii) computational investigations of photocatalytic mechanisms and iii) non-covalent interactions in catalysis. He completed a Swiss European Mobility Program (SEMP) research placement under at Universität Zürich, Switzerland focusing on organic radical intermediates generated through photochemical or tandem electrochemical/transition metal catalysis under the guidance of Prof. Cristina Nevado. He received an EPSRC CDT studentship to conduct his Ph.D. studies within the Technology Enhanced Chemical Synthesis (TECS) center of doctoral training at the University of Bristol, (U.K.).

Jaspreet Kaur was born in India. She received her B.Sc. from the University of Brighton (U.K.) in 2017. In 2020, she received her M.Sc. degree from the Elite Network of Bavaria's Synthesis and Catalysis Master Programme under the supervision of Dr. Joshua P. Barham at the University of Regensburg (Germany). Her research in the Barham group involves i) electron donor-acceptor complexes for catalyst-free photochemical reactions, ii) continuous flow photochemistry and iii) synthetic photoelectrochemistry.

Joshua P. Barham was born in Watford, U.K. He received his industry-based Ph.D. in 2017 under the supervision of Prof. John A. Murphy and Dr. Matthew P. John at the University of Strathclyde and GSK (U.K.), where he i) specialized in the selective radical functionalization of amines *via* single electron transfer and hydrogen atom transfer, and ii) revisited mechanisms of transition metal-free coupling reactions involving alkali metal bases (potassium *tert*-butoxide), showing how organic electron donors formed *in* situ initiated the radical chemistry. His postdoctoral studies with Prof. Yasuo Norikane and Prof. Yoshitaka Hamashima at AIST and the University of Shizuoka (Japan) specialized in flow chemistry and photoredox catalysis. Since 2019 his group has investigated photo-, electro-, photoelectro- and continuous flow organic synthesis at the University of Regensburg, supported by a Sofja Kovalevskaja Award. His group has identified key roles for aggregation states of catalysts/reactants as well as non-covalent catalyst-substrate preassemblies in enabling or diverting photochemical reaction mechanisms. In 2022, he was awarded an ERC Starting Grant.

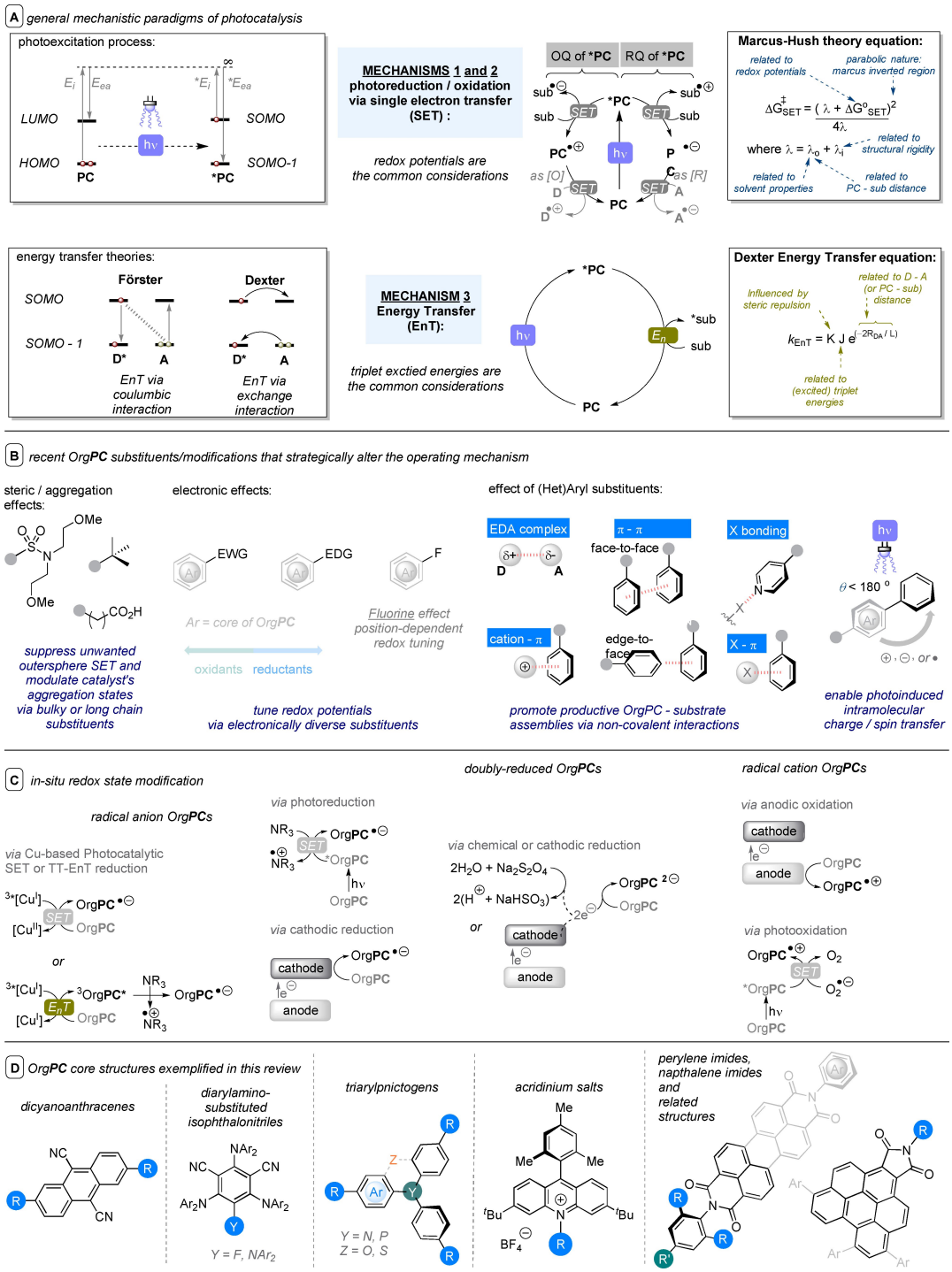

Figure 1. Key concepts in this review. OQ = oxidative quenching cycle; RQ = reductive quenching cycle; E_i = ionization energy; E_{ea} = electron affinity; **D** = donor; **A** = acceptor; **PC** = photocatalyst Org**PC** = Organophotocatalyst; EWG = electron withdrawing group; EDG = electron donating group; X = halogens; Ar = -(Het)aromatic rings which could be mono- or polycyclic with varying substituents; SET = single electron transfer; EnT = energy transfer; TT-EnT = triplet-triplet energy transfer; Asterisks (*) denote photoexcited states.

be beneficial in rational design of photocatalytic reactions or novel catalysts. In other words, one can promote or divert mechanisms by subtle tweaks of the catalyst and/or reaction conditions by considering a more holistic photochemical picture and that is the key message of this review. As aforementioned, organophotocatalysts (Org**PC**s) are modular, and thus enjoy a wide range of possibilities to control or divert their photochemical mechanistic pathways. For instance, the effects of structural modifications on the catalyst's core will be explored (Figure 1B). One approach is the introduction of

substituents which sterically shield and/or electronically influence the Org**PC'**s core, leading to changes in catalyst-substrate interactions as well as the catalyst or reagent's aggregation state. Note that the former affects the kinetics of photochemical processes as the relevant equations (*vide supra*) are distance dependent; in other words, suppression of a pathway can be achieved by 'bulking-up' the Org**PC'**s core. Elsewhere, the modes of aggregation states of catalysts or reactants are often overlooked despite the growing theoretical understanding and application of such phenomena in supramolecular photocatalysis (as reviewed elsewhere).[20] Recent examples of how the changes of aggregation states affect or divert the photochemical mechanism are discussed later in this review. Another approach is the introduction of groups which favor non-covalent interactions (e.g., electron donor acceptor or EDA complex formation, $\pi - \pi$, cation $- \pi$ and halogen bonding interactions) between the Org**PC** and its target substrate, providing the benefit of short intermolecular distances (and improving the rates of photochemical processes, *vide supra*). This is the concept of 'preassembly' or 'precomplexation,' where the catalyst and substrate binds before photoexcitation and it is gaining further evidence and recognition as: i) it overcomes diffusion barriers by diverting reaction kinetics from a bimolecular intermolecular reaction to a 'pseudo-unimolecular/intramolecular' reaction through a static quenching regime; ii) it allows access to higher energy but ultrashort-lived excited states (e.g. accessing excited states higher than the first excited state in an 'anti-Kasha fashion' *vide infra*); iii) it influences regioselectivity and chemoselectivity (i.e. provides tolerance to other redox sensitive functionalities).

Another key strategy that diverts organophotocatalytic mechanisms is manipulating redox states prior to photoexcitation (Figure 1C). This renders a common closed-shell photooxidant as a powerful open-shell photoreductant and *vice versa*. Open-shell (radical species or radical ions) photoredox catalysis can be accessed *in situ* by a co-photocatalyst ('dual-PRC'), by an initial photoredox event (consecutive photoinduced electron transfer, 'conPET'), or by electrochemistry (electro-activated photoredox catalysis, 'e-PRC'). Doubly-reduced Org**PC**s (dianions) can also be generated by photochemical SET or by ground state chemical reduction. While the nature of open-shell photocatalysts was questioned due to their ultrashort excited state lifetimes,[21,22] sophisticated spectroscopic techniques have confirmed their active role in the reaction.[21,23] Moreover, conditions that induce a pseudo-unimolecular electron transfer such as high concentration of reactants (*vide infra*), or Org**PC** catalyst design that drives an organized preassembly (*vide supra*), have enabled the development of a new generation of Org**PC**s and a conceptually different approach to planning organophotocatalytic reactions.

This review is by no means intended to be an exhaustive collection of all Org**PC**s and we recognize excellent and comprehensive precedents.[6–12,24,25] We also note that assembly controlled catalyst-free photochemical reactions are reviewed in detail elsewhere.[26] Instead, this review aims to promote a mechanistic driven understanding with the discussions of recent developments in the field. Thus, we examine five catalyst core groups (Figure 1D) where structural and redox state modifications outlined above have profound effects on their aggregation states, abilities to assemble with target substrates, and thereby directly influence their photochemical mechanistic pathways. We therefore generally exclude examples where assemblies/aggregation states enable photochemical reactions but: i) are not catalytic (e.g. assemblies of stoichiometric partners, i.e. the term Org**PC** is not applicable), ii) where structural information on the assemblies is not yet available (i.e. tailing or no obvious UV-vis absorptions) or iii) where profound differences on diverting reactive pathways are not obvious. Finally, since the focus of this review is on Org**PC** design, we exclude examples involving microstructured solvation effects on aggregation states / EDA complexes. With the ensuing discussions, not only can readers appreciate which catalysts worked for specific reactions, they can identify common patterns and underlying principles in Org**PC** design or *in situ* modifications applicable for future studies and planning of photoreactions.

2. Core structures, modifications, and their effects on photochemical mechanisms

To understand how structural and / or redox modifications affect Org**PC**s' mechanism, the following sections are broken down by the catalyst core. The 'default' reactivity of each Org**PC** core is discussed followed by key reports on core modifications and structure-activity-relationships. Key recurring patterns and trends are highlighted and wherever appropriate, used to build links between similar mechanistic findings in other studies. Being that catalyst-substrate preassembly is one of the major themes of this review, reports that exploit this phenomenon were collected and compared. In some studies, especially where excited state lifetimes render outer-sphere SET unfeasible, interactions between catalyst and substrate were examined using density functional theory (DFT) calculations at an acceptable level of theory for modelling non-covalent interactions *between charged or partially-charged species* (i.e. functional with advanced dispersion corrections; for more information, see Supporting Information (SI)). When redox potentials are given, these are by default referenced *vs.* Saturated Calomel Electrode (SCE). We define 'super' redox agents as those with potentials exceeding ± 2.5 V *vs.* SCE, as these (generally) cannot be accessed by the energy of a single photon excitation regime.

2.1. Dicyanoanthracenes

9,10-Dicyanoanthracene (**DCA**) is a commercially available yellowish crystalline compound which can be prepared by cyanation of 9,10-dibromoanthracene **1 a**[27] or from anthraquinone **1 b** through a cyanohydrin intermediate (Figure 2).[28] The **DCA** core by itself is a powerful closed-shell excited state photooxidant (Figure 3). Alternative mechanisms usually cannot be excluded and are highly dependent on the employed

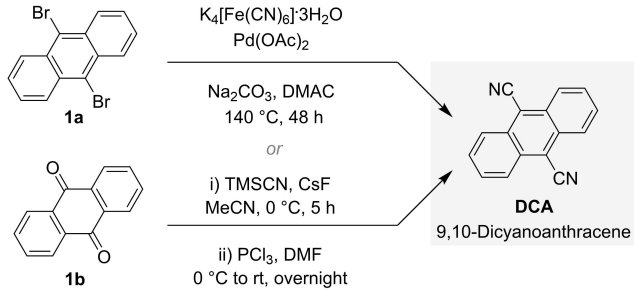

Figure 2. Syntheses of 9,10-dicyanoanthracene **DCA.**

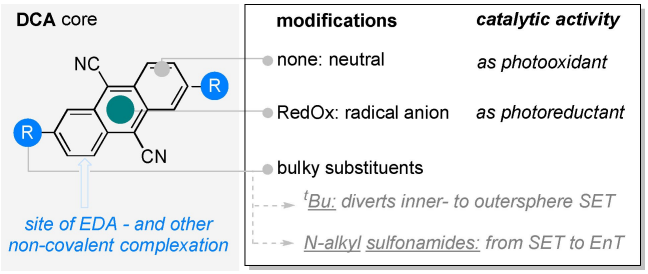

Figure 3. DCA organophotocatalyst core structure, reported modifications and their photocatalytic reactivities.

reaction conditions (*vide supra*). Structural modifications on the core such as: i) introducing bulky groups or ii) functionalized alkyl chains can divert an inner-sphere SET to an outer-sphere one, or even switch the predominant mechanism to EnT. Recently, *in situ* conversion of **DCA** to its radical anion (**DCA**$^{\bullet-}$) switches the default oxidative mechanism to a highly reductive SET pathway. These behaviors will now be discussed in detail.

2.1.1. DCAs as closed-shell SET photooxidants

Intuitively, the combination of an anthracene fluorophore and the electron-withdrawing/visible chromophore-imparting cyano- groups of **DCA** makes the molecule an ideal choice for photooxidations. With an excited state redox potential reaching ($^*E_{1/2}=$) +1.99 V,[29] photoexcited **DCA** (**DCA***) can be quenched by electron-rich molecules by SET. Seminal reports of Schaap and co-workers provided evidence for SET quenching of the photoexcited singlet state of **DCA** (^{1}**DCA***) with diphenylsulfide, olefins, and dioxenes (**2a**–**2d**) by Electron Paramagnetic Resonance (EPR) spectroscopic detection of **DCA**$^{\bullet-}$ and the corresponding radical cations of the substrates (Figure 4).[30] The EPR signal obtained from the chemical quenching of ^{1}**DCA*** was similar to the EPR signals of the electrogenerated radical anion **DCA**$^{\bullet-}$, confirming its formation in the presence of the chemical quenchers.

The photoinduced oxidative SET activity of **DCA** was exploited for several chemical transformations.[31] Notable examples include cycloadditions (*via* 'uphill catalysis')[32] that are challenging to achieve thermally with closed-shell intermedi-

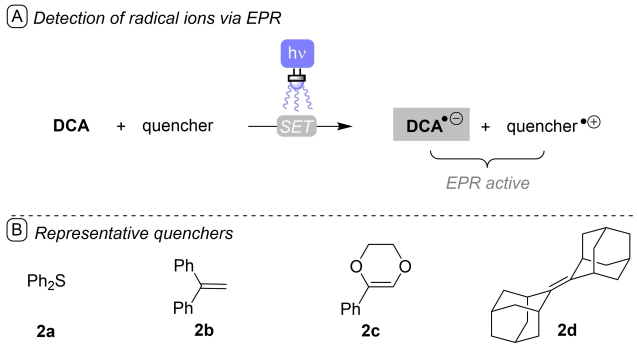

Figure 4. An early study on **DCA** as a photoinduced SET oxidant.

ates (Figure 5). These reactions begin by SET oxidation of a diene (for [4+2]-cycloadditions, Figure 5A,)[33] or of an alkene (for [2+2]-cycloadditions, Figure 5B)[34] by **DCA***, generating the corresponding substrate radical cations. After the addition of the olefin partner, the resulting radical cation is reduced to its neutral form with **DCA**$^{\bullet-}$ closing the catalytic cycle (Figure 5C). We note that recent investigations of reactions akin to photocatalytic [4+2]-cycloadditions revealed a radical chain mechanism, which could also be operative in **DCA** catalyzed systems.[35]

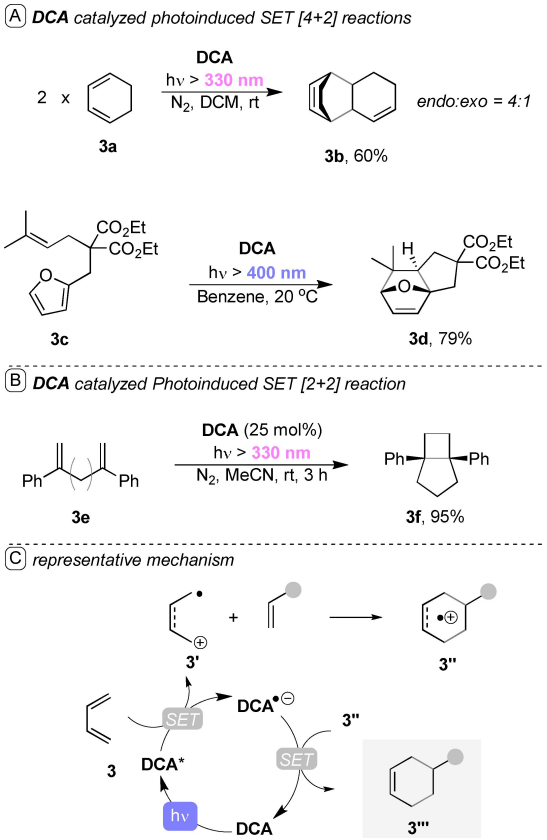

Figure 5. DCA as an SET organophotocatalyst used in cycloaddition reactions.

DCA can also serve as an organophotocatalyst for the formation of carbonyl ylides from diaryl oxiranes. Seminal reports of Whiting and co-workers used this strategy to access oxygen-containing heterocycles by trapping photoredox-generated ylide intermediates from **4a** (in [1,3]-dipolar cycloadditions) with electron poor dipolarophiles (**4b**) (Figure 6).[36] Firstly, **4a** undergoes SET oxidation with **DCA** upon irradiation followed by C–C bond cleavage forming intermediate **4a**$^{\bullet+}$ (where direct irradiation of the oxirane in the absence of **DCA** instead leads to C–O bond cleavage) which then generates the ylide **4a'** by SET from **DCA**$^{\bullet-}$ closing the photoredox catalytic cycle. Dimethyl fumarate **4b** then undergoes [1,3]-dipolar cycloaddition with **4a'** forming the tetrahydrofuran product **4c**, albeit in modest yield.

2.1.2. DCA core: diverting inner-sphere to outer-sphere SET by bulky covalent modification

Considering the utility of tetrahydrofurans as key intermediates for total synthesis strategies toward various lignan natural products, Beeler and co-workers studied the photoredox generation of these heterocyclic substrates (Figure 7).[37] While the reaction using *trans*-stilbene oxide **5a** gave an excellent yield (**5c** >95%) with **DCA**, it failed with substrate **5b** which bears a very electron-rich aromatic substituent (note that in the report of Whiting and co-workers, the substituted tetrahydrofuran yield is low with a slightly electron rich substrate, *vide infra*). They attributed this failure (Figure 7B) to formation of a ylide-**DCA** adduct (**5e**) or formation of an unproductive **5a**–**4b** charge transfer (CT) complex.

They argue that with this CT complex, back electron transfer (BET) is favored over the cage escape of the radical cation of **5b** preventing the productive downstream reaction. Thus, they used **DTAC**, an analogue of **DCA** with two *tert*-butyl groups

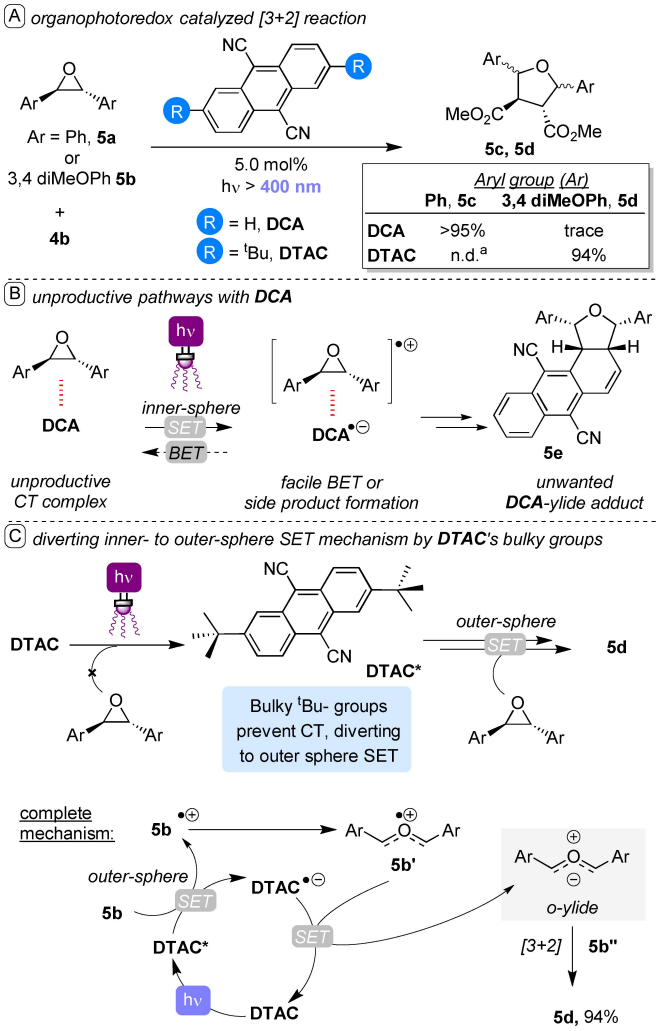

Figure 7. DCA *vs.* **DTAC** as organophotocatalyst for the synthesis of tetrahydrofuran derivatives. [a]n.d. = not determined.

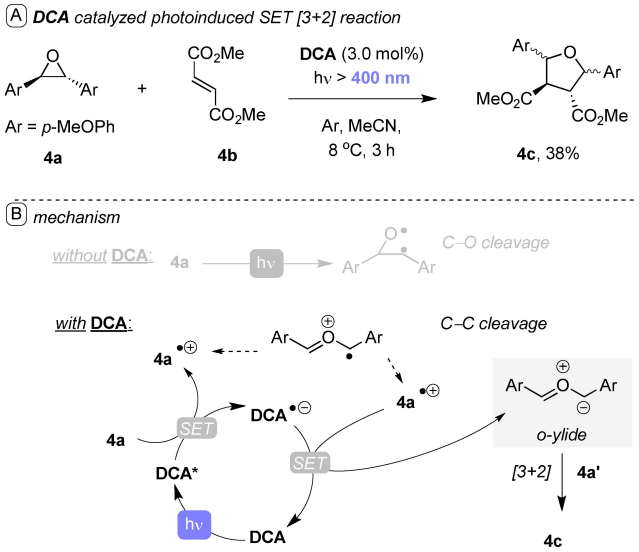

Figure 6. DCA as an SET organophotocatalyst for synthesis of a substituted tetrahydrofuran derivative.

(Figure 7C). Upon introduction of the steric bulk, CT formation was not observed and this diverted the mechanism to an outer-sphere SET affording **5d** in an excellent yield (94%). Computationally (Figure 8, see SI) **5b** forms a more thermodynamically favorable π–π (face-to-face) complex with **DCA** ($\Delta G_{complex} = -2.0$ kcal mol^{-1})[38] than with **DTAC** ($\Delta G_{complex} = 0$ kcal mol^{-1}). Inspecting the optimized geometries of the proposed complexes, the presence of *tert*-butyl groups on **DTAC** disturbed the π planes between the substrate and catalyst which presumably weakened attractive non-covalent interaction between the two molecules. This suggests the repulsive component of London dispersion interactions between *tert*-butyl groups overcome the attractive term under such reaction conditions (polar aprotic solvents).

We also note the possibility that the substrate **5b** is too electron-rich and could push the SET regime with **DCA*** into the Marcus inverted region (where, as the SET becomes more exergonic, the rate of SET becomes slower). In fact, **DCA*** ($^*E_{1/2} = +1.99$ V) has a higher redox potential than **DTAC*** ($^*E_{1/2} = +1.81$ V). Therefore, the lower redox potential of **DTAC*** affects

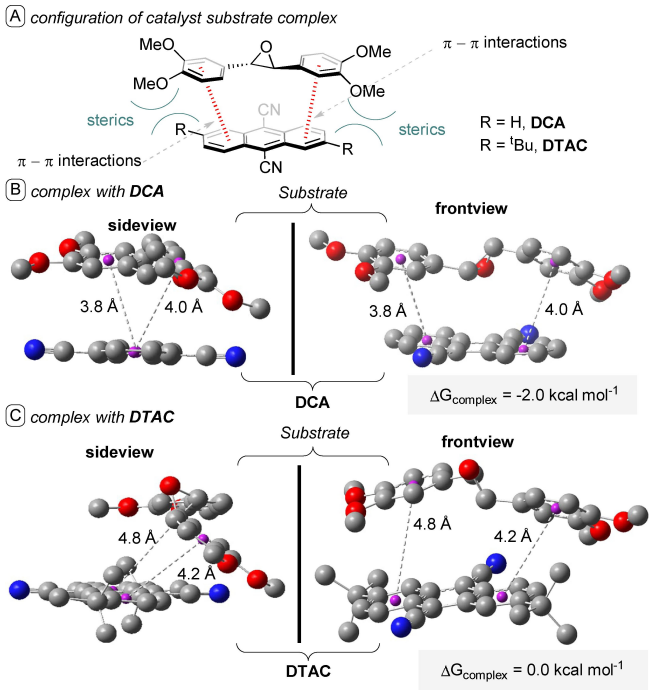

Figure 8. Computational investigation of **DCA** *vs.* **DTAC** complexation with the electron rich stilbene oxide substrate. Calculated using ωB97XD/6-31++g(d,p) level of theory. Centroid-to-centroid distances were defined from the centroids of each individual benzene rings of the substrate to the centroids of the peripheral rings of the catalyst. Color legends: grey = C, red = O, blue = N, magenta = centroid, H atoms are removed for clarity.

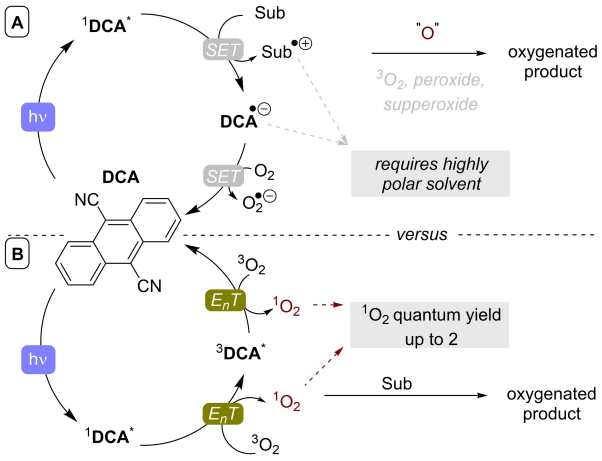

Figure 9. Simplified summary for the divergent pathways for **DCA** catalyzed photo-oxygenations *via* **A)** SET or **B)** EnT. Sub = substrate.

the numerator of the Marcus theory equation (*vide supra*) and may move the photoinduced SET event out of the Marcus inverted region where it is kinetically faster. Furthermore, the computational results mentioned above (loss of rigidity for the **DTAC**-**5 b** complex and a larger separation distance), translate to a larger reorganization energy (λ) component for **DTAC** *vs.* **DCA**. It is known that kinetically-suppressed SET in the Marcus inverted region can be compensated for by an increase of λ.[39] Overall, we favor the assembly disruption argument due to the spectroscopic detection (**DCA**) vs non-detection (**DTAC**) of CT complexes.

2.1.3. DCA core: diverting SET to EnT by bulky covalent modification

Photooxygenation is another reaction class where **DCA** sees wide use as an Org**PC** and exemplifies the dichotomy in the mechanism of **DCA*** (Figure 9). Aside from SET with organic molecules which furnishes radical ion intermediates, energy transfer (EnT) with triplet oxygen ($^3O_2$) is a strongly competitive pathway for **DCA** (and related Org**PC**s)[9] generating singlet oxygen ($^1O_2$). Often, the dominant mechanism is largely determined by factors extrinsic to the catalyst.[40] One of these factors is the nature of medium[41,42] (i.e. solvent polarity,[43] and its O_2 solubility, as well as additive / counterion effects[44]). Generally speaking, productive SET mechanisms are favored in solvents of high polarity.[45] To understand this phenomenon further, consider a general photochemical reaction of an electron rich donor molecule **D** and electron poor acceptor molecule **A** in Figure 10.[45] Upon irradiation, a polar exciplex is formed which has two fates: i) relaxation to the ground state or ii) solvent separation of charged species after SET. The former occurs in non-polar media presumably due to a polarity mismatch as exciplex is polar. The latter is favored in polar medium where the charged species are well stabilized by the solvent and which promotes diffusive cage escape. Efficient solvent cage escape of the radical ions prevents unwanted BET and allows downstream reactions to happen. In some cases however, non-covalent interactions between charged intermediates are too strong even in polar solvents as seen at the onset of Beeler and co-workers' study (*vide supra*).

Singlet oxygen sensitization *via* EnT pathway on the other hand is hardly affected by solvent polarity. In fact, quantum yield measurements by Foote and co-workers for **DCA** sensitized $^1O_2$ generation in both nonpolar (benzene) and polar (MeCN) solvents is $\Phi = 1.5$ with some measurements reaching to *ca.* 2.[46,47] This means about two $^1O_2$ molecules are produced for every photon **DCA** absorbs (implications and applications of this will be discussed in following sections). Santamaria and co-workers reported the use of **DCA** in oxygenated MeCN for *N*-demethylation reaction of dialkylmethylamines such as **6 a** forming ***nor*-6 a** with variable amounts of *N*-formyl **O-6 a** side products (Figure 11).[48] For this reaction, they proposed an SET

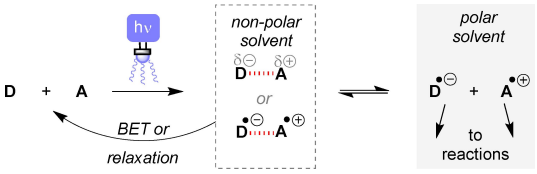

Figure 10. General rationale for the solvent polarity dependence of the SET mechanism.

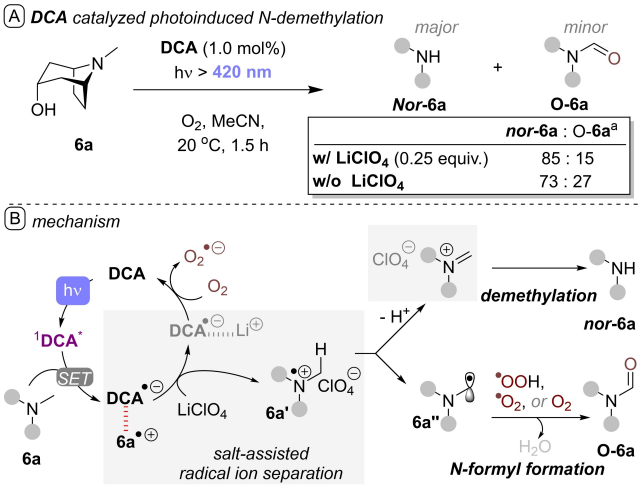

Figure 11. DCA organophotocatalytic *N*-demethylation of dialkylmethylamines. [a] HPLC / ^{1}H NMR product ratio, isolated yields were not specified.

mechanism[49] that is promoted by the addition of $LiClO_4$ as an additive assisting the separation of the radical-ion pair as intermediates. Then, they proposed that **O-6a** formation proceeds directly from an α-amino radical intermediate, while the *N*-demethylation pathway proceeds *via* an iminium ion intermediate stabilized by the ClO_4^- anion. This ion-pairing stabilization was proposed as the reason for the enhanced demethylation over the formation of **O-6a** side products. Highlighting the significance of dialkylmethylamines alkaloids and pharmaceuticals, Barham and co-workers designed an organophotocatalytic procedure based a novel **DCA** derivative that is compatible with enabling continuous flow technology (for scale up and handling ignitable gases safely (Figure 12).[29] Initially, they aimed to address the poor solubility (mg mL^{-1}) of **DCA** in polar aprotic solvents, since solid suspensions are deleterious to the chemistry (in efficient light absorption), its reproducibility (attempts to reproduce the conditions of Santamaria and co-workers gave complex mixtures), and instrumentation (clogging of small diameter tubing). With these considerations, a new generation catalyst called **DCAS** was synthesized from inexpensive anthraquinone (**1b**) starting material. The enhanced solubility *via* covalent modification was achieved by an interplay of two strategies: i) introduction of polar sulfonamide substituents compatible with the solvent[50] and ii) bis-methoxyethyl side chains which disrupt the π–π face-to-face stacking[51] and thus the aggregation state of the **DCA** core (highly organized aggregates promote an SET mechanism, *vide infra*). The solubility of **DCAS** was 6-fold enhanced *vs.* **DCA** while its photophysical properties were largely unaffected. Due to the electron-withdrawing sulfonamide groups, the excited state redox potential of the former ($E_{1/2}$ [^{1}**DCAS***/**DCAS**$^{\bullet-}$] = +2.31 V) was higher than the latter ($E_{1/2}$[^{1}**DCA***/ **DCA**$^{\bullet-}$] = +1.99 V). The authors then employed **DCAS** for regioselective *N*-CH_3 oxidations of trialkylamine-containing alkaloids and pharmaceuticals (Figure 13). Unlike the preceding reports of Santamaria and co-workers, demethylation was hardly observed – a notable shift in downstream chemoselectivity driven by catalyst modification. Taking the thermodynamics, (i.e. excited state oxidation potential) of SET quenching of ^{1}**DCAS*** by the amine substrates at surface value, one may be quick to suggest enhanced performance of ^{1}**DCAS*** is because it is a more potent oxidant. However, it was found that the Stern-Volmer rate constant of quenching of ^{1}**DCAS*** with a given amine substrate is two orders of magnitude smaller than that of ^{1}**DCA*** (Figure 14). Kinetically speaking (corroborated by DFT and Marcus theory calculations), that means the rate of SET from the amine substrate to ^{1}**DCAS*** is slower than that to ^{1}**DCA***.

Further experiments (Stern Volmer quenching rates of O_2 *vs.* amine, ^{18}O-isotope labelling, chemical trapping of $^1O_2$, and the inhibitory effect of adding a physical quencher of $^1O_2$) suggested that singlet oxygen sensitization is favored for the **DCAS** catalyzed photooxidation. In summary, the modification of **DCA** core with the alkylsulfonamide substituents diverted the mechanism from SET to EnT by: i) suppressing SET by

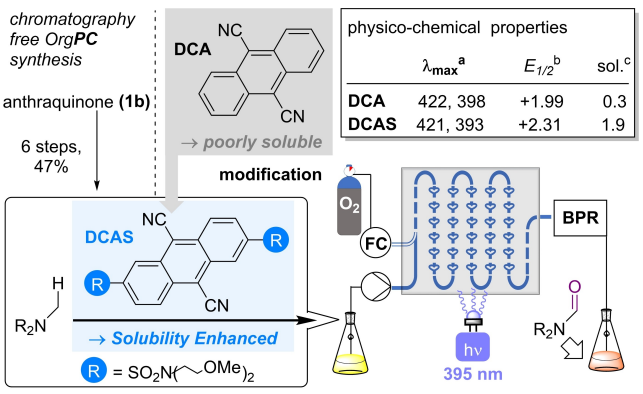

Figure 12. DCAS catalyst and flow reaction design. [a] nm, UV-Vis spectra; [b] V, $E_{1/2}$(^{1}**PC***/**PC**$^{\bullet-}$) *vs.* SCE; [c] mg mL^{-1} solubility in MeCN.

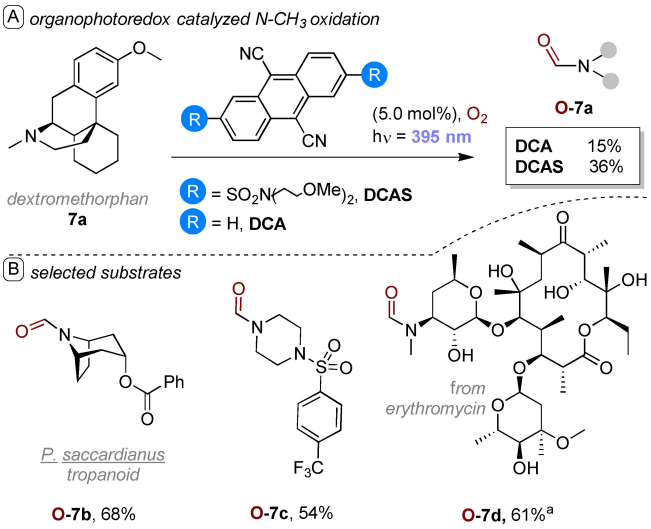

Figure 13. DCAS organophotocatalytic late-stage *N*-CH_3 oxidation of pharmaceutically-relevant dialkylmethyl amines. [a] ^{1}H NMR yield.

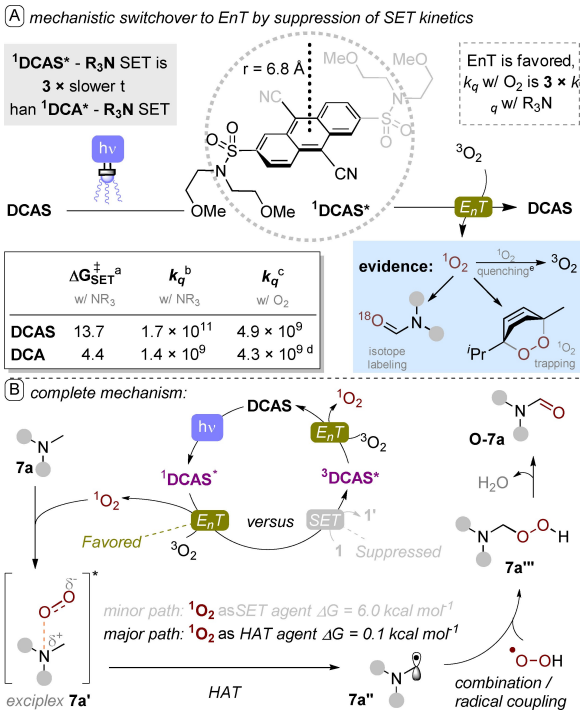

Figure 14. A) **DCAS** diverting mechanism from SET to EnT. [a] Calculated using DFT and Marcus theory, units in kcal mol^{-1} ; [b,c] Stern Volmer quenching rate constant in M^{-1}; [d] value obtained from the literature[42,47] [e] DABCO is a known $^1O_2$ physical quencher.[52] B) Final proposed mechanism.

increasing the activation energy barrier ($\Delta G^{\ddagger}_{SET}$) for **DCAS** due to its larger external reorganization energy than **DCA** (this is brought about by **DCAS**' larger size or molecular radius *vs.* **DCA**) and ii) suppressing the interaction between the amine and **DCAS**' redox active core by steric bulk (or by adopting a different aggregation state vs **DCA**) biasing the system instead toward interaction with the small O_2 molecule. As the SET is suppressed, O_2 sensitization takes over as the dominant pathway.

Then the reaction proceeds *via* complexation of $^1O_2$ with amine **7a** followed by HAT (this is exergonic while the plausible alternative – SET between the amine and $^1O_2$ – is endergonic), radical coupling of **7a''** with HOO$^{\bullet}$ radical, and finally, dehydration of **7a'''** affording the product **O-7a**. We note that in this case it is not as simple as concluding that the diversion of mechanism toward EnT is due to a 'de-aggregation' of the **DCA** core by the alkylsulfonamide substituents, since the single photon counting decay profile (lifetime measurements) revealed that **DCAS** may adopt a different type of aggregation state.[29] Elsewhere, it is known that J-type aggregates of **PDI**s divert their excited state mechanism toward EnT (*vide infra*).

2.1.4. DCA core redox state modification: diverting oxidative to reductive mechanism

So far, the EnT and SET pathways for **DCA** were discussed. In both cases, the active catalytic species are generated upon the irradiation of the neutral closed-shell molecule. There is an alternative mode of electron transfer reactivity for oxidative Org**PC**s akin to **DCA** that proceeds *via* their radical anions, generated by *in situ* redox modifications (Figure 15). In fact recently, there has been an influx of studies exploiting the use of radical ion species as photocatalysts with the key motivation of accessing redox potentials beyond the limit of traditional photoredox catalysis and beyond what is typically achievable with single photons.[53–55] As mentioned, potent organophotooxidation catalysts yield vividly colored radical anions in solution upon reduction, which upon irradiation of light are super reductants (and *vice versa* for organophotoreduction catalysts forming upon oxidation, super oxidizing radical cation organophotoatalysts, *vide infra*). Therefore, from a mechanistic point of view, the modification of **DCA**'s redox state to **DCA**$^{\bullet-}$ *via* SET is a mode of diverting mechanistic pathways.

There are a few reports in which *in situ*-generated **DCA**$^{\bullet-}$ was proposed as a photocatalyst for reductions of aryl halides (chlorides and bromides **8**) to aryl radicals (Figure 16 and 17). For example, the groups of Jacobi von Wangelin, Pérez-Ruiz,

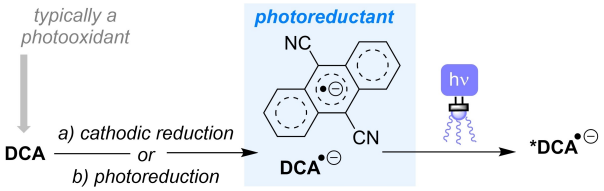

Figure 15. *In situ* redox modification of **DCA**.

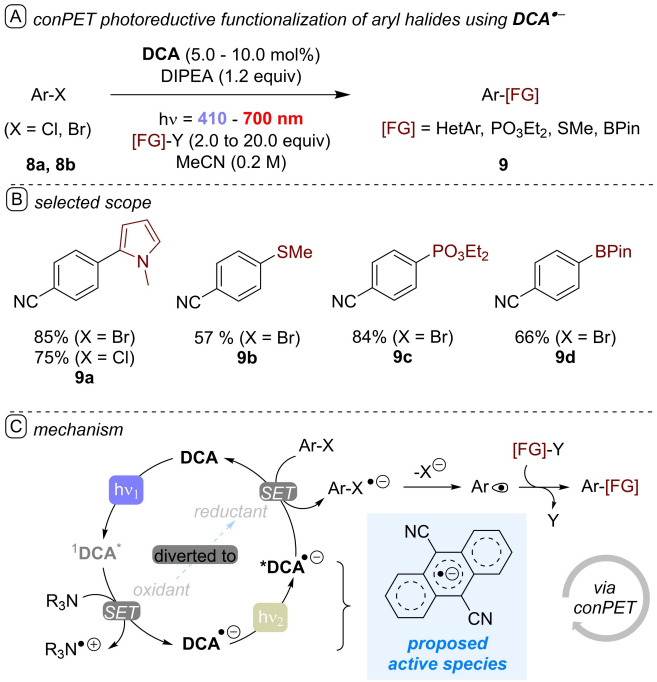

Figure 16. A) **DCA**$^{\bullet-}$ as a (super) reductive organophotocatalyst. B) Ar–X functionalization, selected scope. C) *In situ* generation of active open-shell species *via* conPET catalytic cycle.

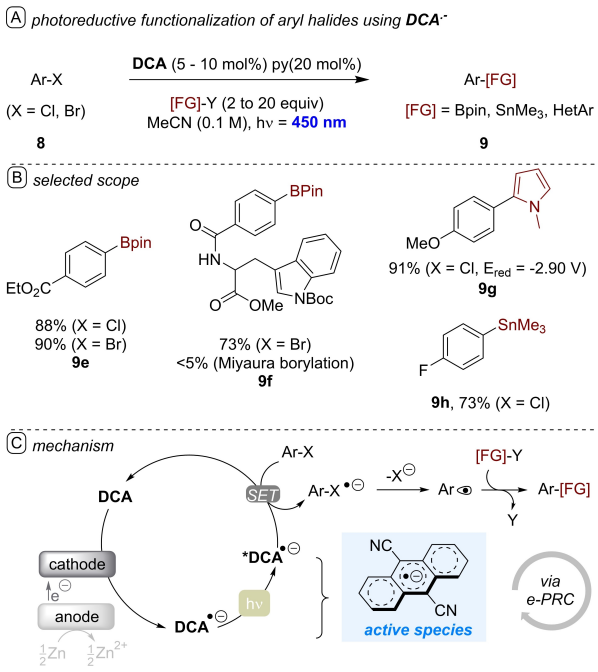

Figure 17. A) **DCA**$^{\bullet-}$ as a (super) reductive organophotocatalyst, py = pyridine. B) Ar–X functionalization, selected scope. C) *In situ* generation of active open-shell species *via* e-PRC catalytic cycle.

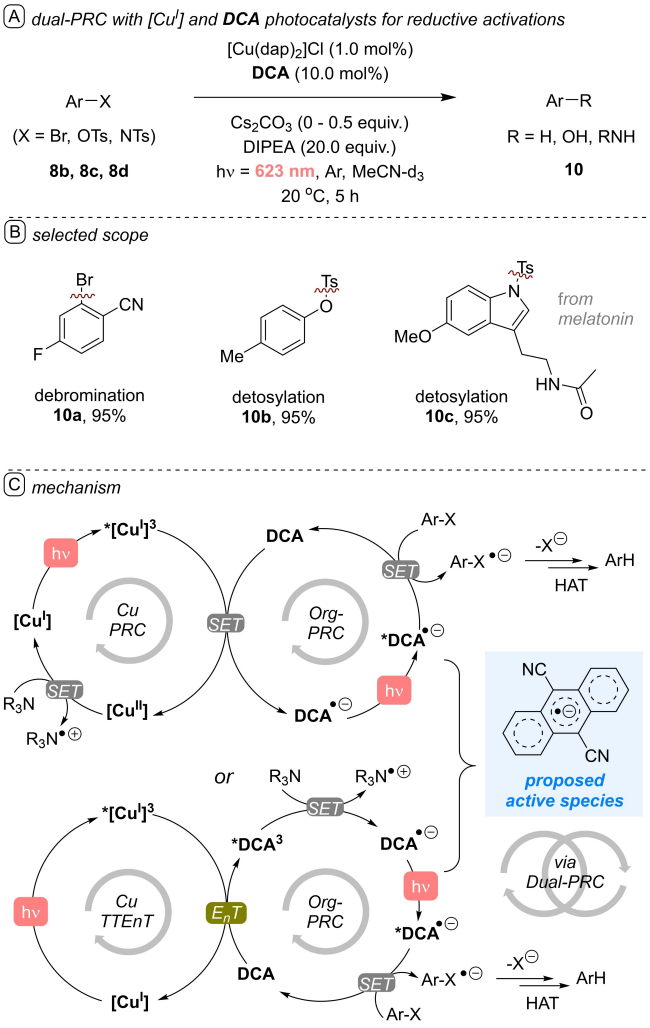

Figure 18. A) Dual-PRC with a [**Cu**^{I}] photocatalyst and **DCA**$^{\bullet-}$ as a reductive Org**PC** used for B) dehalogenation and detosylation reactions, selected scope. C) *In situ* generation of active open-shell species *via* a dual-PRC catalytic cycle.

and co-workers[56] used a biphotonic process in one catalytic cycle, now popularly known as consecutive photoinduced electron transfer (conPET),[57] where **DCA**$^{\bullet-}$ is first generated photochemically (**DCA** absorbs at the blue region, *ca.* 420 nm) using di-*iso*-propylethylamine (DIPEA) as a sacrificial SET reductant (Figure 16). Then, **DCA**$^{\bullet-}$ is excited by a second photon of light (it absorbs in the green region >500 nm) generating the ***DCA**$^{\bullet-}$ as a super reductant. On the other hand, Lambert, Lin and co-workers[58] used cathodic reduction to generate **DCA**$^{\bullet-}$ replacing the first photoredox step and the use of sacrificial reductants when compared with conPET (Figure 17). This technique is known as electrochemically-mediated photoredox catalysis (e-PRC).[54,55] In both cases, the generated aryl radical was intercepted by various functional groups and such procedures allowed transition metal-free coupling of C(sp^2)–X with –C(sp^2), -[S], -[P], -[Sn], or -[B]-containing functionality.

In a recent study, Wenger and co-workers employed dual photoredox catalysis (Dual-PRC) to access the open-shell **DCA**$^{\bullet-}$ organophotocatalyst from an initial [Cu^{I}]-based photoredox catalyst (Figure 18).[59a] This dual-PRC strategy is unique compared to previous reports on conPET for two reasons: i) it utilizes low energy red photons, which are less invasive and less energy-intensive than blue photons typically used in PRC but have higher penetration depth even in relatively opaque media; ii) it uses two catalysts to shuttle the photon energy, a phenomenon in part resembling the Z-scheme of natural photosynthesis. The strategy was used for debromination, detosylation, and deacylation under mild conditions. Key to the success of their mechanism is the [Cu^{I}]-cycle to **DCA**-cycle SET. Alternatively, they proposed a triplet-triplet energy transfer (TTEnT) between the [Cu^{I}]-cycle and **DCA**-cycle may be plausible. In their more recent study, they found out that changing the photosensitizing partner of **DCA** to an [Os^{II}] complex allowed the normal oxidative reactivity of **DCA** using red light (not shown).[59b] While the synthetic utility of reductively-activated, photoexcited **DCA** is established, the actual involvement of open-shell ions (radical anions or cations) in the catalytic cycle was a subject of discussion, due to the ultrashort lifetimes of these species in their photoexcited states. Non-radiative decay of photoexcited radical ions is usually faster than diffusion, precluding bimolecular quenching events. For ***DCA**$^{\bullet-}$ a 13.5 ns[60] excited state lifetime has been claimed thus leading Lambert, Lin and co-workers to propose it undergoes reductive SET by standard bimolecular quenching in their e-PRC study.[58] However, due to mismatches between the UV-Vis of the (brown) electrogenerated species[58] and that of chemically-prepared (purple) **DCA**$^{\bullet-}$,[61] others suggested that this lifetime

value instead belongs to a decomposition by-product of **DCA**$^{\bullet-}$.[22b,62] It was shown how **DCA**$^{\bullet-}$ reacts readily with O_2 to form a cyanoanthrolate, a likely candidate for this nanosecond lifetime.[61,62] Recent experiments by Vauthey and co-workers[21] measured the lifetime of **DCA**$^{\bullet-}$ directly by transient electronic absorption spectroscopy (TAS) and confirmed **DCA**$^{\bullet-}$ indeed has an ultrashort excited state lifetime (~3 ps; similar to other photoexcited radical ions that live in the picosecond domain).[54] Nevertheless, it was pointed out that radical ion photocatalysis is feasible even with such an ultrashort-lived excited state if the substrate concentration is high enough (usually >0.3 M) that SET quenching becomes static. Alternatively, a pseudo first-order SET quenching can be promoted by non-covalent preassembly of **DCA**$^{\bullet-}$ with the substrate (Figure 19). Although Lambert, Lin, and co-workers did not detect a non-covalent interaction *via* UV-vis spectroscopy of **DCA**$^{\bullet-}$ in the presence of a target substrate,[58] unfortunately the UV-vis spectrum measured likely belongs not to **DCA**$^{\bullet-}$ in the first place but rather to a cyanoanthrolate species. Calculations find a weak interaction ($\Delta G_{complex} = -0.7$ kcal mol^{-1}) between the π-planes of catalyst **DCA**$^{\bullet-}$ and chlorobenzene as a model substrate (see SI). Although quadrupolar repulsion between the planes[63] seems to be enhanced due to the anionic nature of **DCA**$^{\bullet-}$, this is presumably overcome by van der Waals interactions due to the relatively large surface area of the anthracene core.[64] As the excited state molecular orbitals are populated over the entire ***DCA**$^{\bullet-}$ plane[21,58] and are sandwiched between the catalyst and the substrate in the proposed preassembly, a pseudo-intramolecular SET would ensue. The presence and crucial benefit of similar non-covalent preassemblies to open-shell photocatalysis (i.e. surmounting ultrafast excited state dynamics and accessing 'anti-Kasha' higher energy states SET)[65–68,69] were proven and highlighted in other studies (*vide supra*).

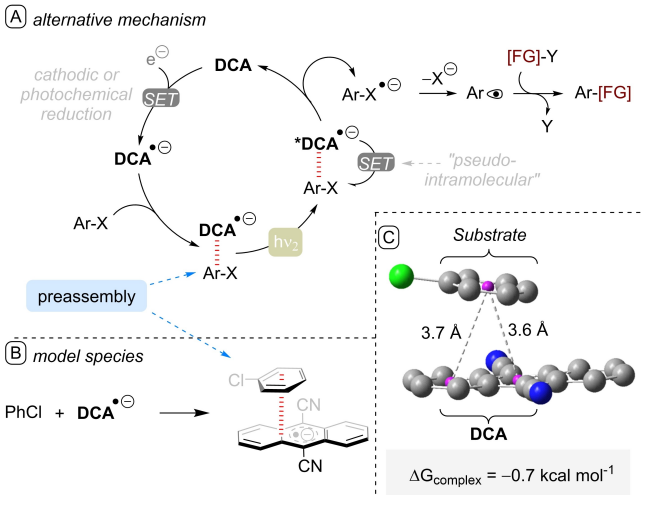

Figure 19. A) Exploration of alternative preassembly-assisted photoreduction using ***DCA**$^{\bullet-}$. B) Model species: preassembly for **DCA**$^{\bullet-}$ and chlorobenzene B) Computational investigation of the preassembly, calculated using ωB97XD/6–31++g(d,p) level of theory. Centroid-to-centroid distances were defined from the centroid of the substrate's benzene ring to the centroids of the middle and peripheral rings of **DCA**$^{\bullet-}$. Color legends: grey = C, blue = N, green = Cl, magenta = centroids, H atoms are removed for clarity.

2.2. 4CzIPN and other isophthalonitrile derivatives

1,2,3,5-tetrakis(carbazol-9-yl)4,6-isophthalonitrile (**4CzIPN**, and related compounds) is a yellowish solid which can be prepared (Figure 20) by a straightforward S_NAr reaction of carbazole (Cz, **11**) and 2,4,5,6-tetrafluoroisophthalonitrile.[70,71] Although originally developed as efficient OLED[72] and TADF materials,[25] Zhang and co-workers noticed the potential of these donor-acceptor dyads in photoredox catalysis.[70] Isophthalonitrile organophotocatalysts have gained popularity in a growing number of applications[73] owing to: i) their spatial HOMO–LUMO separation which makes it easy to tune the catalyst redox properties (Figure 21) ii) their wide redox windows (*vs.* other Org**PC**s) allowing them to function as cost effective alternatives to Iridium complexes. Photooxidant pathways are enhanced with structural modifications that affect the isophthalonitrile acceptor fragment (where the ground state LUMO is located) while photoreductant pathways can be enhanced by tweaking the electronics of the diarylamine donor fragments (where the ground state HOMO is located). **4CzIPN** and its derivatives were also reported to effect highly reducing open-shell photocatalysis by irradiation of their *in situ* generated radical anions.[74,75]

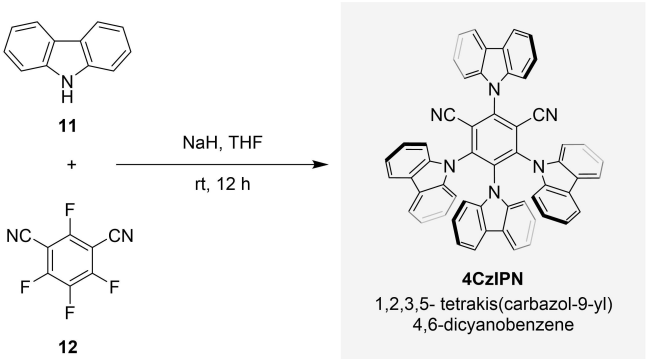

Figure 20. Synthesis of 1,2,3,5-tetrakis(arbazole-9-yl)4,6-isophthalonitrile (**4CzIPN**).

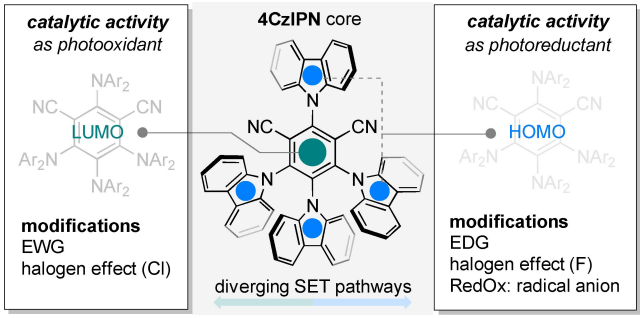

Figure 21. 4CzIPN organophotocatalyst core structure, reported modified derivatives and their photocatalytic reactivities.

2.2.1. 4CzIPN and its derivatives as neutral state photooxidants

Considering the distinct LUMO and HOMO locations for **4CzIPN**, at the acceptor isophthalonitrile fragment and at the donor carbazole fragment respectively, Zeitler and co-workers studied the effects of structural modifications on each fragment.[76b] By itself, **4CzIPN** is an oxidative Org**PC** (Figure 22) which is capable of oxidizing substrates *via* its ground-state radical cation ($E_{1/2}$(**PC**$^{\bullet+}$/**PC**) = +1.49 V). This is generated by prior oxidative quenching of its excited state by an electron acceptor **A** in the oxidative quenching photoredox cycle (OQ-PRC) or directly with its neutral photoexcited state *via* a reductive quenching photoredox cycle (RQ-PRC, $E_{1/2}$(**PC***/**PC**$^{\bullet-}$) = +1.43 V). When the carbazole at the 5th position is replaced by Cl (**3Cz(Cl)IPN**), the oxidizing power is enhanced (both *via* OQ-PRC and RQ-PRC). Furthermore, Deibel and co-workers showed that the presence of Cl in **3Cz(Cl)IPN** increased the charge transfer characters of its excited states and decreased the singlet to triplet energy gap.[76b] **4CzIPN** is popularly used for redox neutral reactions[25] such as decarboxylative conjugate (Giese) reaction (*via* RQ-PRC) (Figure 23A).[76] On the other hand, bromination of electron-rich anisole can be achieved using **3Cz(Cl)IPN** *via* OQ-PRC (Figure 23B).

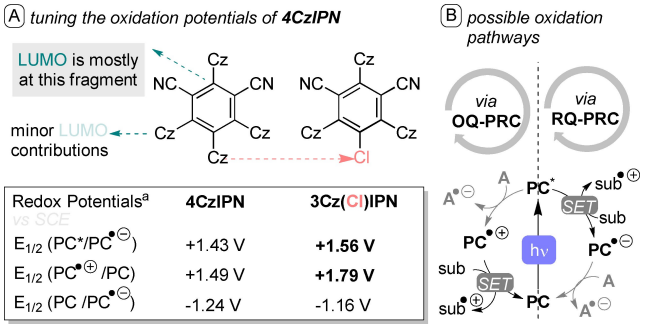

Figure 22. 4CzIPN organophotooxidation catalyst. A) Tuning redox potentials *via* halogen (Cl) effect. B) Possible pathways for substrate oxidation. OQ-PRC = oxidative quenching photoredox cycle, RQ = reductive quenching photoredox cycle, Cz = carbazole, [a] in MeCN (0.1 M $^{n}Bu_4N{\cdot}BF_4$).

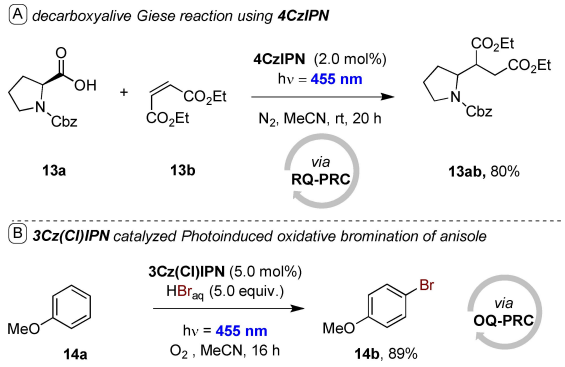

Figure 23. Examples of **4CzIPN** and **3CzClIPN** as oxidative organophotocatalysts *via* A) Reductive quenching cycle (RQ-PRC) or B) Oxidative quenching cycle (OQ-PRC).

Waser and co-workers considered the effect of halide substituents at the carbazoyl fragment with the reasoning that Cz substituents at the 4- and 6- positions contribute minimally to the ground state LUMO of the catalyst (Figure 24).[77] With a series of **4(X$_2$Cz)IPN** derivatives, they found out that the excited state redox potential $E_{1/2}$(**PC***/**PC**) follows an increasing trend with different X substituents: H < F < Cl < Br. They also found considerable structural distortions for the derivatives with X=Cl and Br. While **4(Br$_2$Cz)IPN*** was the most potent oxidant, they employed the more soluble **4(Cl$_2$Cz)IPN** for a fragmentative alkynylation of cyclic oxime ether **15a** with phenylethynylbenziodoxolones (Ph-**EBX**) like **15b**, affording **15c** (Figure 25). Chen, Yu, and co-workers[78] reported the use of **4(t Bu$_2$Cz)IPN** as Org**PC** for the proton-coupled electron transfer (PCET) phosphorylation of isocyanides such as **16a** (Figure 26). While the rationale for the *tert*-butylated catalyst's efficiency is not fully explored in their study, it is possible that the bulky groups

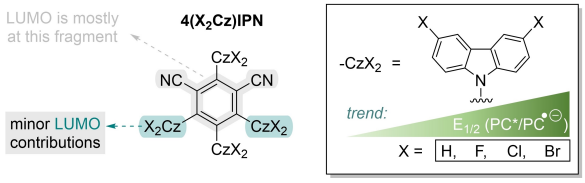

Figure 24. 4CzIPN as an oxidative organophotocatalyst: effect of halide substituent at carbazoyl (Cz) moiety.

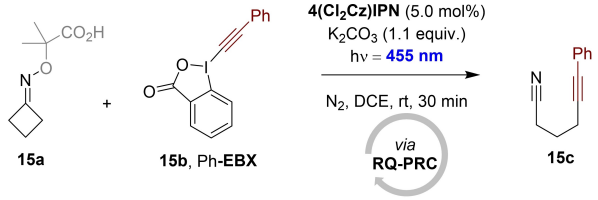

Figure 25. 4(Cl$_2$Cz)IPN as an oxidative organophotocatalyst for a fragmentation-alkynylation of a cyclic oxime ether.

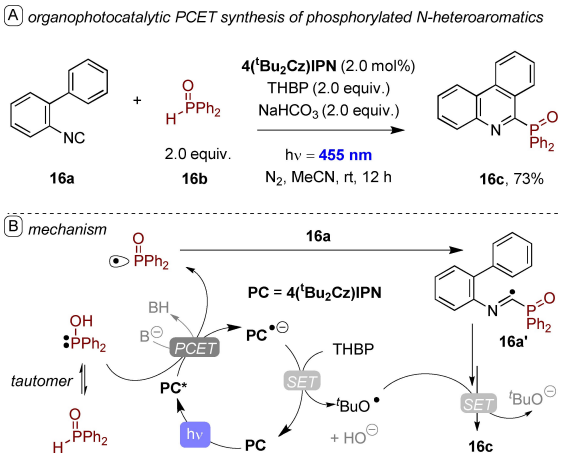

Figure 26. 4(t Bu$_2$Cz)IPN as a reductive organophotocatalyst for the synthesis of phosphorylated *N*-heteroaromatics. PCET = proton coupled electron transfer.

prevent known photocatalyst bleaching pathways (i.e. similar to the reported photosubstitution of the -CN group with C-centered radicals discovered by König and co-workers).[79]

2.2.2. 4CzIPN and its derivatives as neutral state photoreductants

The radical anion generated by the RQ-PRC of **4CZIPN** is a potent reductant (Figure 27). Considering that the HOMO of **4CzIPN** is situated at its carbazoyl fragments, Zeitler and co-workers investigated the effect of changing them to a stronger electron donor; a diphenylamine fragment.[76] Moreover, they reported an unprecedented F atom effect which further enhanced the reducing capacity of the catalyst. Of the three catalysts shown in Figure 27, **3DPA2FBN** yields the most potent reductant ($E_{1/2}$(**PC**/**PC**$^{\bullet-}$) = −1.92 V in DCM). This catalyst also gave the best yields for sequential (C–O cleavage then C–C coupling) photo-reductive transformations of lignin derivatives to pinacols (Figure 28).

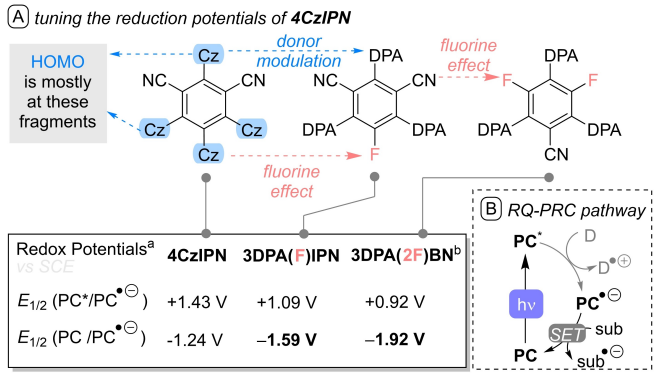

Figure 27. 4CzIPN as a reductive organophotocatalyst. A) Tuning redox potentials *via* donor modulation or fluorine effect. B) Reduction *via* RQ-PRC = reductive quenching photoredox cycle. Cz = carbazole, DPA = diphenylamine, [a] in MeCN (0.1 M $^{n}Bu_4N{\cdot}BF_4$). [b] measured in DCM.

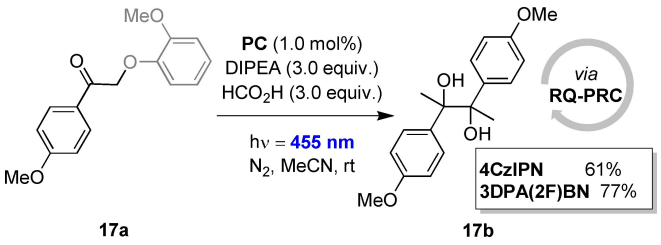

Figure 28. Example of **4CzIPN** and **3DPA(2F)BN** as reductive organophotocatalysts *via* an oxidative quenching cycle (OQ-PRC) for transformation of lignin derivative to pinacol.

2.2.3. 4CzIPN and its derivatives as radical anion super photoreductants

Wickens and co-workers accessed a highly potent reducing agent from **4DPAIPN** by photoexciting its radical anion generated *in situ* by cathodic reduction.[74] With this catalyst, they demonstrated reductive C(sp^2)–N cleavages of *N,N,N*-trialkylanilinium salt **18a** or C(sp^2)–O cleavages of aryl dialkyl-phosphates such as **18b** (Figure 29). While replacement of the functional group with H atoms was the main topic, the generated aryl radicals could also be intercepted in phosphorylations, borylations, or heteroarylations. In a follow-up study, Wickens and co-workers revealed that when sodium formate is used for the photocatalytic generation of radical anions, the carbon dioxide radical anion ($CO_2^{\bullet-}$) is generated as a non-innocent species (Figure 30)[80] that is capable of chemical reduction of **4DPAIPN** to its active radical anion state. Alternatively, $CO_2^{\bullet-}$ can engage in direct chemical reduction of certain aryl halide species.

Zhuo, Wu, and co-workers demonstrated that ***4CzIPN**$^{\bullet-}$ can also be harnessed as a 'super' photoreducing open-shell organophotocatalyst through a conPET mechanism.[75] In their study, they reported that substituting one carbazole unit with ethylphenyl amine (**3CzEPAIPN**) improved catalytic activity as catalyst bleaching was suppressed (Figure 31). With this catalyst, they were able to generate aryl radicals from **8a** which were then intercepted by -[B] or -[P] functional groups forming **20a**–**20d**. They were able to obtain **20d** in continuous flow with a productivity of 13.1 g day^{-1}. Furthermore, they were able

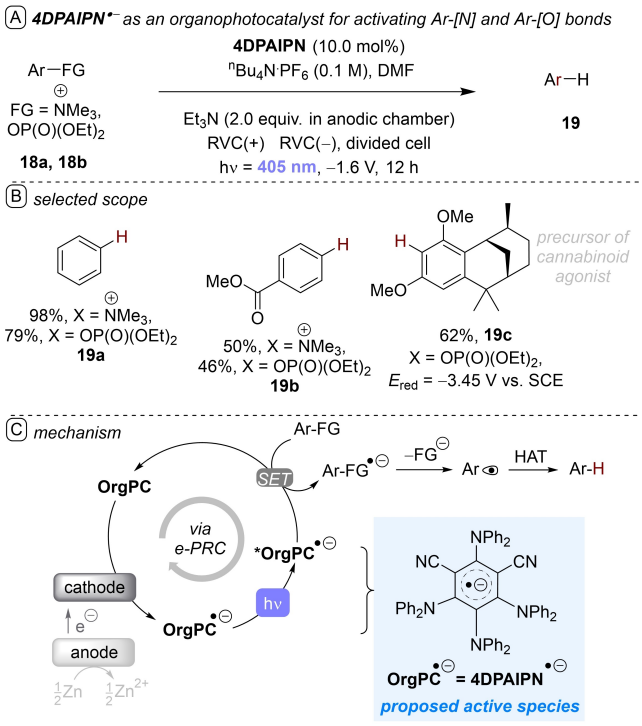

Figure 29. 4DPAIPN$^{\bullet-}$ as a reductive organophotocatalyst. A) reductive cleavage of anilinium salt C–N bonds and arylphosphonate C–O bonds by e-PRC. B) selected scope. C) e-PRC mechanism.

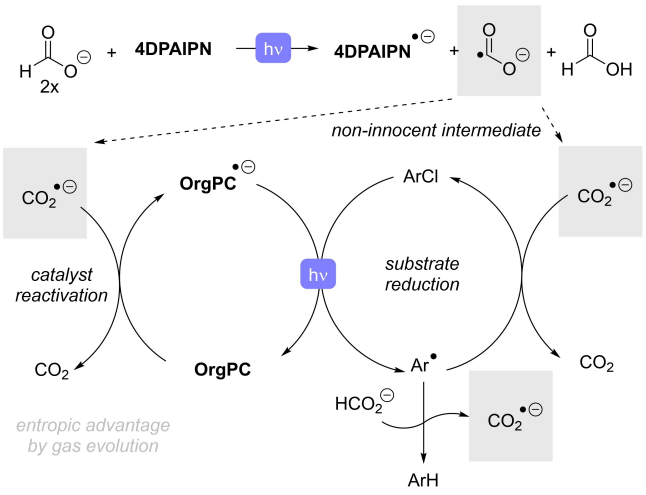

Figure 30. Role of non-innocent intermediates in **4DPAIPN** open-shell photocatalysis.

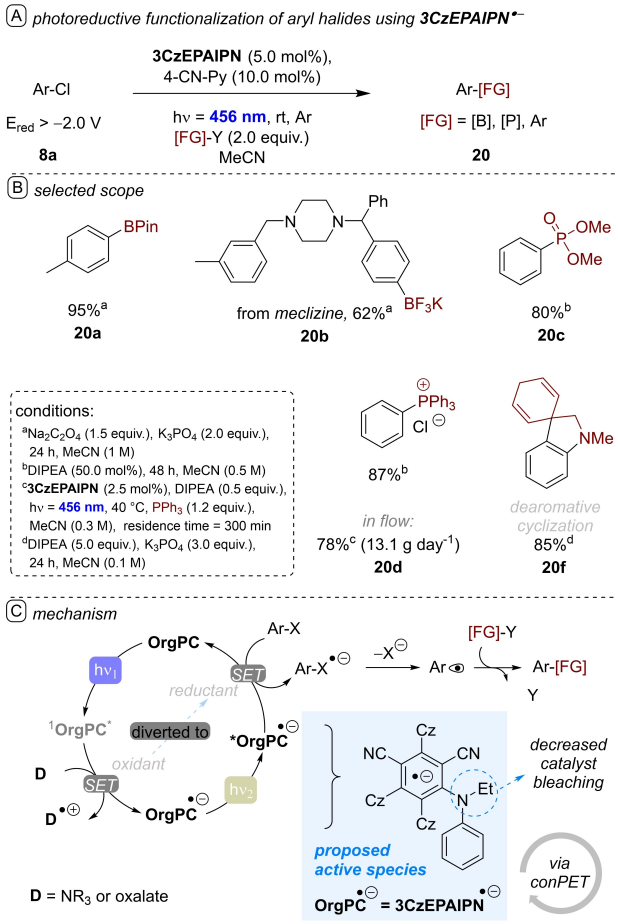

Figure 31. A) **3CzEPAIPN**•− as organophotoreducing catalyst used for B) Ar–Cl functionalization, selected scope. C) *in situ* generation of active open-shell species *via* a conPET catalytic cycle. Cz = carbazole.

to trap these aryl radicals with a pendant phenyl group intramolecularly, forming spiro compounds such as **20f**. We note the precedent of Jui and co-workers using dearomative hydroarylation to access these spiro compounds from aryl halides using **3DPAFIPN**.[81]

Inspired by the stability and redox properties of **3CzEPAIPN**, Vega-Peñaloza, Dell'Amico and co-workers synthesized analogues of **3CzEPAIPN**, with different substituents at the carbazole moieties. They discovered that the electron-rich derivative **3[(MeO)$_2$Cz]EPAIPN** has significant absorbance reaching up to 496 nm and bears a redox window ($E_{1/2}$(**PC**$^{\bullet+}$/**PC***) = −1.49 V; $E_{1/2}$(**PC***/**PC**$^{\bullet-}$) = +0.98 V) which can effect photoreductions under one photon conditions (not shown).[82]

2.3. Perylene and naphthalene imide derivatives

Perylene diimides (**PDIs**), naphthalene diimides (**NDIs**), naphthalene monoimides (**NMIs**) and their derivatives are polyaromatics fused with imides (Figure 32A) which usually bear *N*-aryl functionality (for the latter two classes bearing *N*-phenyls, these are often abbreviated as **NpDI** or **NpMI**). **PDIs** are well known for their thermal stability and photostability as well as their redox and optical properties which found applications in a wide range of areas such as: dyes, electronic materials (e.g. as n-type semiconductors), photovoltaics, photoreceptors, and (together with their smaller **NDI** and **NMI** cousins) synthetic photochemistry and photoelectrochemistry.[66,83] These molecules are typically synthesized by condensing their constituent carboxylic acid anhydride with aromatic or aliphatic amine components. As an example, the synthesis of di-*iso*-propyl-containing **NpMI** from **21a** and **21b** is shown in Figure 32B.[89] Upon photoexcitation of their neutral states, these compounds can act as photooxidants but the photochemistry of their

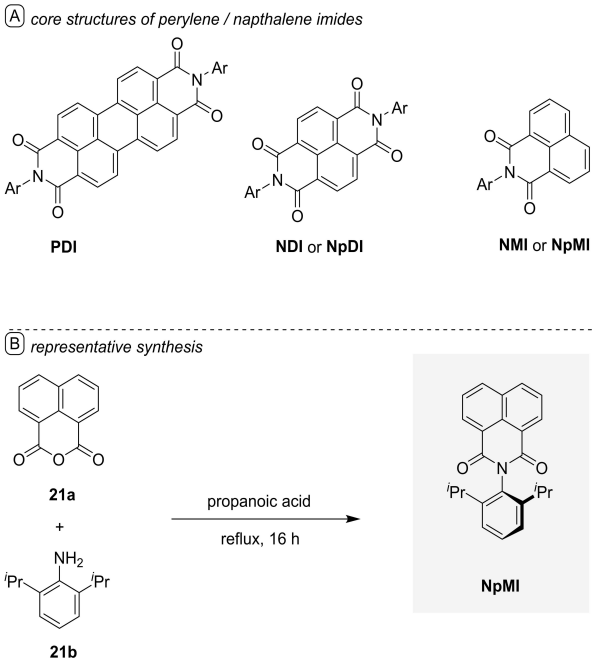

Figure 32. A) Core structures of perylene / naphthalene imides **B.) NpMI** as a representative for synthesis of perylene and naphthalene imide derivatives.

radical anions as potent photoreductants is more popular[84] (Figure 33). Key structural modifications thus far are on the *N*-aryl moiety, focusing on fragments that alter CT, promote solubility, alter self-aggregation states or promote preassembly with a target substrate which further enhance the reactivity on the radical anion.

2.3.1. Perylene diimides supramolecular photocatalyst: diverting SET to EnT by control of aggregation states

Closed-shell **PDI** supramolecular nanofibers exhibit photooxidant properties allowing phenol degradation or H_2O oxidation to be carried without any need of metal based co-catalyst.[85,86a] The mechanism is heavily influenced by the self-aggregation behavior of the **PDI** core which is in turn influenced by the nature of the substituents attached to *N* (Figure 34). Zhu, Wang and co-workers showed that **PDIs** with short polar side chains (*N*-alkyl carboxylic acids) form organized H-aggregates (H-**PDI**) through π–π face-to-face interactions (Figure 34B, left).[86] The HOMO-LUMO gap of **PDI** becomes lower due to such π-stacking interactions and this sets up conduction and valence bands (CB and VB) with a narrow band gap (1.69 eV) as it forms the aggregate. Together with the induced electric field brought by the polar *N*-alkyl carboxylic acids (converted to carboxylate to promote further aggregation and catalysis), H-**PDI** reacts as a semi-conductor SET photocatalyst which upon photoexcitation generates holes (h^+) at the VB where H_2O oxidation occurs, and promotes electrons at the CB where reduction of O_2 to superoxide occurs.[85,86b] Interestingly, Zhu, Guan, and co-workers demonstrated the mechanism changes to EnT when the aggregation state adopts J-aggregates (J-**PDI**). Long chain *N*-alkyl carboxylic acids induce a lateral displacement of the π planes. J-**PDI** sensitizes the formation of $^1O_2$ ($\Phi = 0.66$) under red light irradiation, which could be applicable to cancer treatment research given that $^1O_2$ can induce cancer cell death.[86b] While the distinct mechanism for these species is not yet fully understood, Zhu, Guan, and co-workers pointed out that it is primarily not due to thermodynamics as EnT should be both favorable for H-**PDI** and J-**PDI**.[86b] Nevertheless, this observation, that the introduction of long alkyl groups modified both the aggregation state and mechanism, is consistent with other Org**PC**s such as **DCAS** (*vide supra*).[29]

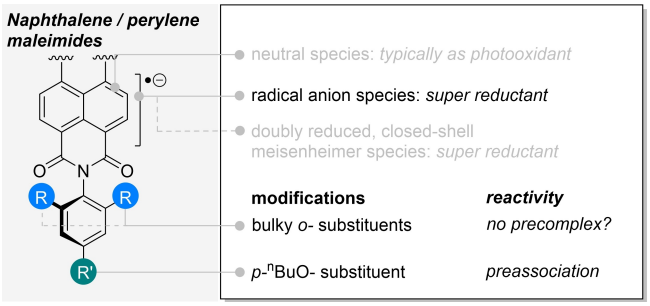

Figure 33. Naphthalene maleimide organophotocatalyst core structure, reported modification strategies and their photocatalytic reactivities.

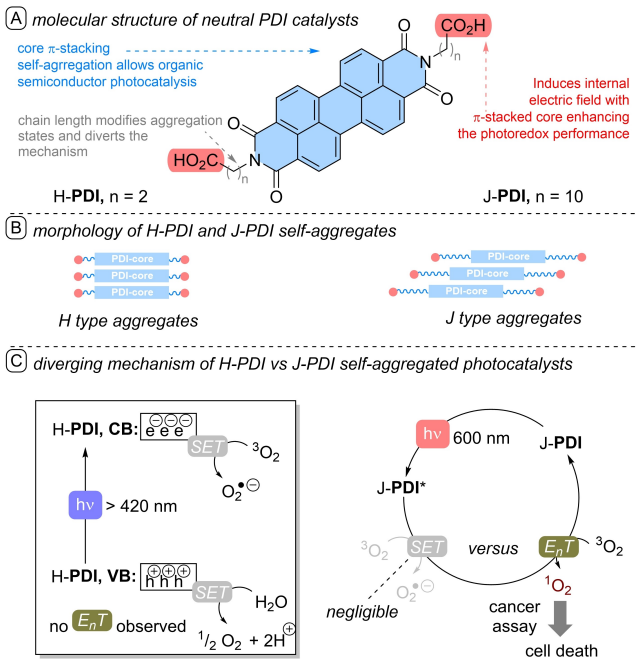

Figure 34. A) Perylene diimide organophotocatalyst core structure, reported modification strategies and their photocatalytic reactivities. B) morphology of aggregates. C) divergent mechanisms for H-type and J-type aggregates.

2.3.2. Perylene diimides core redox state modification: diverting oxidative to reductive mechanism

Pioneering efforts of König and co-workers explored conPET reduction of aryl halides (Figure 35).[57] They employed perylene diimide (**PDI**) as a conPET catalyst to harness the energy from two visible light excitations. First, excitation of **PDI** using 455 nm and its reductive quenching results in **PDI**$^{\bullet-}$ which is further excited with a second photon of light (also with 455 nm LEDs) to give ***PDI**$^{\bullet-}$. conPET process allowed to reduce aryl iodides, bromides and chlorides which cannot be achieved with single photon excitation as the redox potential ($E_{1/2}$) of **PDI**/**PDI**$^{\bullet-}$ is −0.37 V whereas the reduction peak potential (E^p_{red}) of aryl iodides, bromides and chlorides is −1.59 V to −2.90 V.[58,87] Once the substrate is reduced to ArX$^{\bullet-}$, fragmentation of ArX$^{\bullet-}$ gives an aryl radical which can either abstract a hydrogen from $Et_3N^{\bullet+}$ or from the solvent to give reduced products, or can be trapped using unsaturated partners for C−C coupling.

Wenger and co-workers employed an aqueous-soluble **PDI** (Figure 36) with polyethene glycol side chains (**PDI-PEG**) in which its dianionic species has an improved reducing ability $E_{1/2}$ (***PC**$^{2-}$/**PC**$^{\bullet-}$) = −2.65 V) over previously conPET-based **PDI**$^{\bullet-}$ $E_{1/2}$ (***PC**$^{\bullet-}$/**PC** = −1.87 V).[88] They initially formed the dianion **PDI-PEG**$^{2-}$ using a chemical reductant $Na_2S_2O_4$, either in a biphasic H_2O–MeCN mixture containing a phase transfer reagent, or in aqueous solution. **PDI-PEG**$^{2-}$ is then photoexcited in a single photon regime ($h\nu = 525$ nm) in contrast to the two photon regime ($h\nu = 455$ nm) of conPET. These luminescent PDI dianions have longer excited state lifetimes (*ca.* 6 ns). Photo-

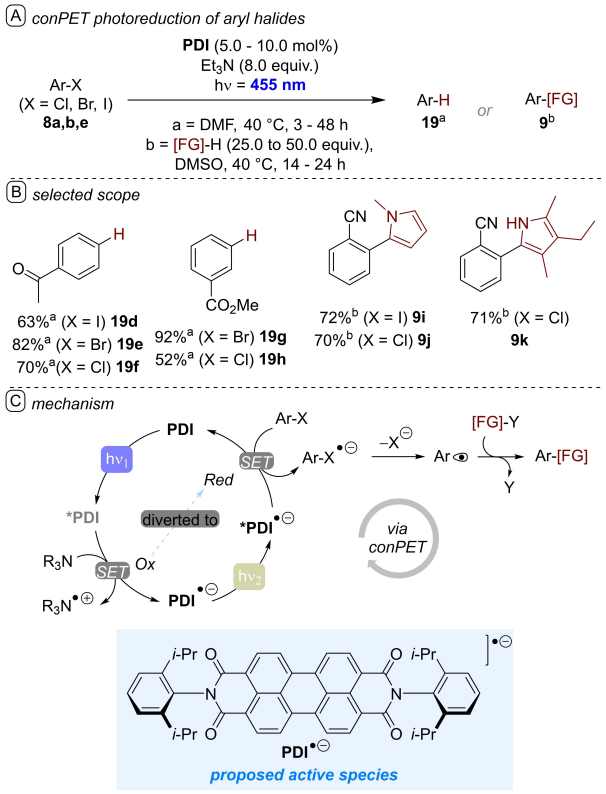

Figure 35. A) **PDI**$^{\bullet-}$ as a reducing organophotocatalyst. B) Ar–X reduction and functionalization, selected scope. C) mechanism *via* a conPET catalytic cycle.

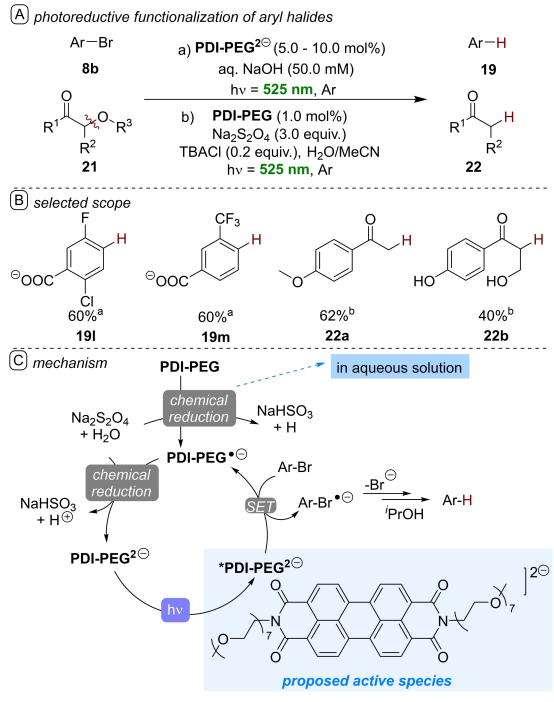

Figure 36. A) **PDI-PEG**$^{2-}$ as a potent reductive Org**PC** for reductive debromination and C–O cleavage in H_2O. B) selected scope. C) mechanism.

excited **PDI**$^{2-}$ dianion was then used for reductive debrominations in aqueous media and for reductive C(sp^3)–O bond cleavages of lignin-related model substrates in a biphasic H_2O-MeCN mixture using a phase transfer agent.

Elsewhere, inspired by the work of König and co-workers, Würthner, Xie and co-workers have demonstrated how carboxyphenyl-substituted **PDI**s (**cp-PDI**s) can be charged consecutively with triethanolamine (TEOA) in a conPET-type manner to **cp-PDI**$^{2-}$ which when loaded onto Pt-doped TiO_2 culminates in a highly photoactive hydrogen evolution reaction material.[83f] In their study (not shown), π-stacking aggregation of neutral **cp-PDI** was observed, and it was proposed that the further reductive PET from TEOA to **cp-PDI**$^{\bullet-}$ must occur by a preassembly given the ultrashort lifetime of ***cp-PDI**$^{\bullet-}$ (145 ps, measured by transient absorption spectroscopy) prohibiting diffusion-controlled reductive quenching. Indirectly supporting this notion, the authors demonstrated dynamic proton exchange between TEOA and (neutral) **cp-PDI** by NMR spectroscopy.

2.3.3. Naphthalene imide radical anion 'super' photoreductants

The discovery of **PDI**$^{\bullet-}$ as a strong photoreductant inspired further studies on the application of other photoexcited radical anions, such as naphthalene-based analogues, smaller congener of **PDI**s. Wickens and co-workers discovered that **NpMI** is superior as a precatalyst for the e-PRC reductive debromination of aryl halides *vs.* **PDI** and **NDI** (Figure 37),[89] ***NpMI**$^{\bullet-}$ is more reducing than ***PDI**$^{\bullet-}$ and ***NDI**$^{\bullet-}$.[66] Interestingly **PhMI**, which has a smaller aromatic core, gave inferior yields despite having roughly similar redox properties with **NpMI** suggesting that the reaction with **NpMI** benefits from precomplexation (especially, given that the lifetime of 20 ps ***NpMI**$^{\bullet-}$ is ultrashort). After establishing electron-primed, photoexcited **NpMI** as an excellent photoreductant, they explored the reduction of electron-neutral and electron-rich aryl halides. Cathodic reduction of **NpMI** (under constant current electrolysis) results in colored **NpMI**$^{\bullet-}$ which is then photoexcited to reduce aryl chlorides with reduction potentials as deep as −3.4 V. Resulting aryl radicals are engaged to yield radical coupling products, such as phosphorylation and (hetero)arylation.

2.3.4. Radical anion decomposition products as active photocatalysts?

Cozzi, Ceroni and co-workers investigated the role of ***PDI**$^{\bullet-}$, in conPET reactions.[22a] Their spectroscopic (reaction profile monitoring) and electrochemical investigation show that ***PDI**$^{\bullet-}$ has an ultrashort lifetime and suggests that a non-isolated photodecomposition product of **PDI** was responsible for the activation of the aryl bromides. The evolution of EPR signal (the loss of hyperfine interaction) suggested that the decomposition product exhibits less symmetry, or the electron is delocalized over a larger surface area *vs.* the original **PDI**. Such investigations highlight the importance of deeper mechanistic

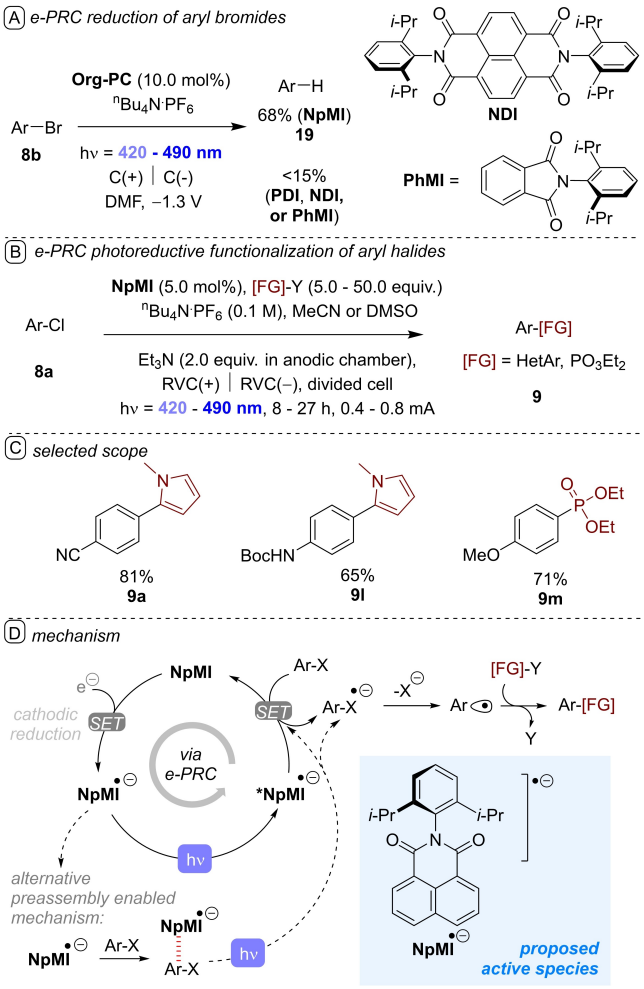

Figure 37. A) **NpMI**•⁻ as a (super) reductive organophotocatalyst. B) Ar–X reduction and functionalization. C) mechanism *via* e-PRC catalytic cycle.

investigations on photochemical reactions, particularly on elucidating whether decomposed photocatalyst species are active catalysts.[22] Nonetheless, questions remain whether the photoexcited radical ion or the decomposed product is the main catalytically-active species (see Section 2.3.3). We note Lupton's comprehensive study providing spectroscopic evidence for conPET[65] and that the participation of ultrashort(ps)-lived photoexcited radical ions has been confirmed in other photochemical reactions, enabled by a substrate assembly.[66–68]

The ultrashort lifetimes of doublet excited states (in the picosecond domain) such as ***NpMI**•⁻ had also puzzled Nocera and co-workers, who wondered if a closed-shell decomposition product of the catalyst could be catalytically active.[22b] In their investigation of **NpMI**•⁻ photocatalysis, they revealed that at applying a constant potential of −3.0 V (a potential magnitude *ca.* double that used by the groups of Wickens[89] or Barham[66]) forms a species with a UV-vis absorption consistent with a chemically-prepared *ortho*-[**NpMI**(H)]⁻ anion. They proposed that this acts as a closed-shell Meisenheimer complex super reductant (Figure 38). This species has a singlet emissive lifetime of 20 ns. They proposed that such species is the one responsible

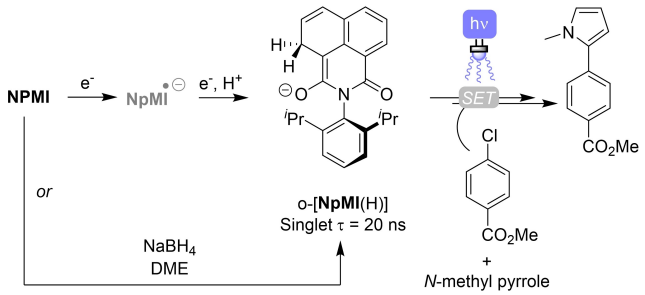

Figure 38. Probing the possibility of *ortho*-[**NpMI**(H)]⁻ as the photoactive species in **NpMI** e-PRC reactions.

for the previously reported photoredox chemistry of **NpMI**, originally proposed by Wickens and co-workers to involve ***NpMI**•⁻.[89] However, the studies of Vauthey and co-workers[21] and Lee, Cho, You and co-workers[23] provide clear evidence of radical anions as photoactive species by transient absorption spectroscopy, confirming that a substrate preassembly can rationalize catalytic activity of the ultrashort-lived excited state radical ion. Indeed, the redox power of the closed-shell photoexcited Meisenheimer complex was inferior to ***NpMI**•⁻ and as such it only engaged 'activated' chloroarenes with electron-withdrawing groups in appreciable rates. The Wickens group subsequently showed by kinetic analysis how there are *two* active forms of the **NpMI** catalyst during the reaction of 4-chlorobiphenyl, the latter being less active than the former.[74] Therefore, while the Meisenheimer complex is undoubtedly a photoactive species, it is not necessarily clear if it is the one responsible for catalytic activity in the study of Wickens and co-workers, or potentially catalytic activity involves multiple catalytically-active intermediates.[74,89] Nonetheless, the study of Nocera and co-workers[22b] is critically important in prompting practitioners to carefully consider whether what they add to the reaction is actually the active catalyst, or whether it is a precursor to the active catalyst.

Barham, König and co-workers[66] introduced another analogue of naphthalene monoimide, *N*-(*para*-butoxyphenyl)naphthalene monoimide (**ⁿBuO-NpMI**). **ⁿBuO-NpMI** promoted the reduction of phosphinates of aliphatic alcohols which effects cleavage of the C(sp^3)–O bond (Figure 39). The catalytic cycle is similar to the one with **NpMI**; after the reduction of phosphinates ($E^p_{red} \approx -2.4$ to -2.6 V) by the photoexcited *[**ⁿBuO-NpMI**•⁻], C(sp^3)–O bond cleavage occurs to form a C(sp^3) carbon radical which likely further transforms into a C(sp^3) carbanion after downstream cathodic reduction. Elimination of an α- leaving group (chloride, bromide) results, overall, in reductive olefination similar to the Corey-Winter olefination. If no leaving group is present adjacent to the carbanion, overall deoxygenation occurs in a Barton-McCombie fashion. It is noteworthy that both **ⁿBuO-NpMI** and **NpMI** have similar UV-vis properties (in their neutral and radical anion forms) and ground state reduction potentials ($E_{1/2} = -1.3$ V). Despite these similarities, aryl halides were tolerated when Barham and co-workers employed **ⁿBuO-NpMI** in comparison to the reported reduction of aryl halides by Wickens and co-

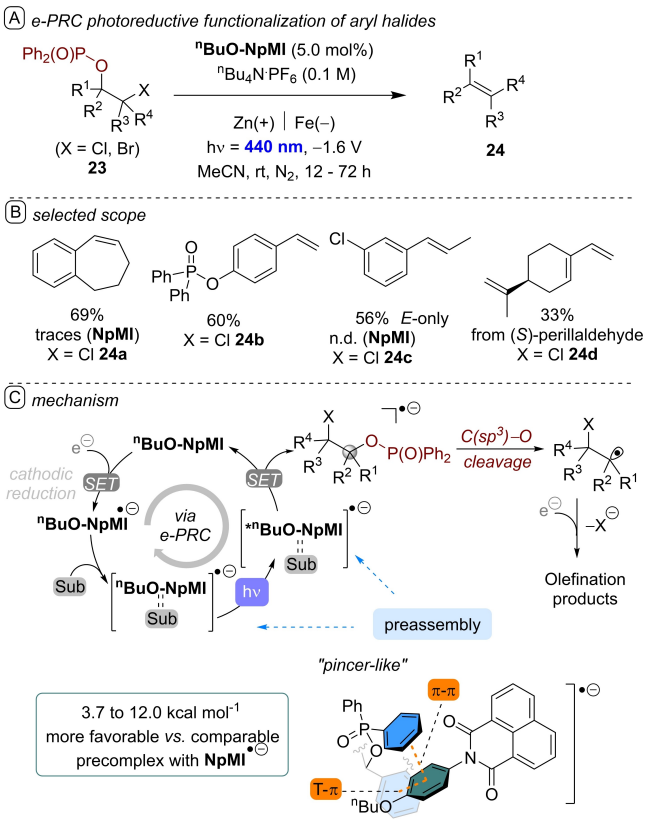

Figure 39. A) **^{n}BuO-NpMI$^{\bullet-}$** as a (super) reductive organophotocatalyst for Corey-Winter-like olefination. B) selected scope. C) mechanism *via* e-PRC catalytic cycle.

workers using **NpMI**, though the redox potentials of aryl halides (E^{p}_{red} of chloro- and bromobenzene is −2.78 V and −2.44 V, respectively) and phosphinates ($E^{p}_{red} \approx -2.4$ to −2.6 V) are similar. Another difference observed by Barham and co-workers is that **^{n}BuO-NpMI** worked better for all (benzylic/allylic) substrates whereas **NpMI** was not successful for these substrates.

Barham, König and co-workers proposed non-covalent preassembly on the *N*-Aryl fragment explained the reactivity and chemo-selectivity brought by **^{n}BuO-NpMI**.[54] While there were no obvious spectroscopic (EPR, UV-vis) perturbations when treating **^{n}BuO-NpMI$^{\bullet-}$** with a target substrate (that would be confirmative of preassembly), the preassembly was evidenced indirectly by using computational studies and structure activity relationship investigations (i.e. varying the catalyst structure). The C(sp^3)–O cleavage was found to be rate-determining by comparison of experimental redox potentials, computational BDFEs and product yields. Taken together with the success of **^{n}BuO-NpMI** *vs.* the failure of **NpMI**, this suggests that preassembly is the phenomenon by which only **^{n}BuO-NpMI** can influence the rate-determining C(sp^3)–O cleavage.

Elsewhere, Miyake and co-workers reported the use of a benzo[ghi]perylene (**BPI**) photoredox catalyst (Figure 1D) that engages in a modified conPET cycle in the presence of hydroxide base (not shown).[69b] Upon photoexcitation, the authors showed how ***BPI$^{\bullet-}$** engages arenes in Birch-type reductions, but not from the first excited state. Miyake and co-workers proposed either i) formation of solvated electrons, that requires photoexcitation of **BPI$^{\bullet-}$** to higher excited states or ii) a ground state preassembly of **BPI$^{\bullet-}$** and arene substrate which engages in photoreduction of the arene component from a higher excited state (in an anti-Kasha fashion). The catalyst was seemingly unstable to the reaction conditions, since successive portion-wise addition was required. Given that the chemistry reveals selective reduction of aromatic systems (E^{0}_{red} (PhH) = −3.66 V[90]) in the presence of amides/carbamates (E^{0}_{red} *ca.* −2.50 V[90]), the ability to selectively reduce arene moieties supports the authors' latter proposal and this is in line with the selective reduction of arene moieties over esters reported in an earlier study of Tuttle, Murphy and co-workers using UV-photoexcited stroichiometric organic electron donors for selective Birch-type debenzylation reactions.[90] In both cases, π-stacking interactions between the photoactive species and arene prior to photoexcitation are likely operative, and were studied using DFT calculations by Tuttle, Murphy and co-workers.[90]

2.4. Triarylpnictogens

Triarylpnictogen-type photocatalysts either contain the more common Nitrogen (and related heterocycles) or Phosphorous as the central atom. The key synthetic step to access triarylamines is the transition metal-catalyzed arylation of mono- or diarylamines (Figure 40A).[91] Triarylphosphines on the other hand, are synthesized from white phosphorous P_4 industrially *via* a two-step process: chlorination followed by alkali metal (Na) reductive arylation with ArCl (Figure 40B).[92] Recent efforts of Wolf and co-workers, allowed a mild and direct procedure to access triarylphosphine and tetraarylphosphonium salts from P_4 *via* photocatalysis.[93] Triarylamines and triarylphosphines are neutral state photoreductants (Figure 41). When SET oxidized to their radical cations, the reactivity of triarylamines can be shifted to ground-state oxidants or excited state superoxidants. The aryl substituents are sites for π–π or cation–π interactions that are enhanced by larger or extended aryl systems (i.e. naphthalene or biphenyls) which are critical in realizing open-

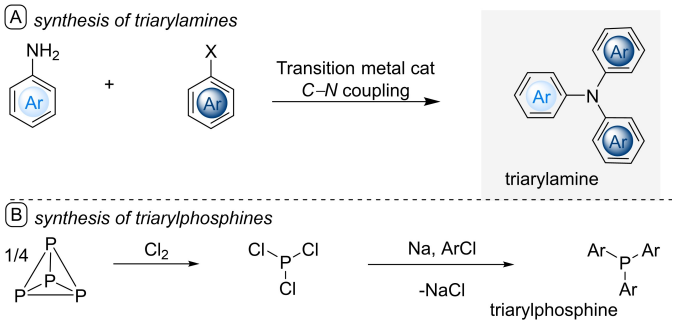

Figure 40. Key synthetic strategies to access triarylpnictogen cores. A) typical access to triarylamines. B) synthesis of triarylphosphines from P_4.

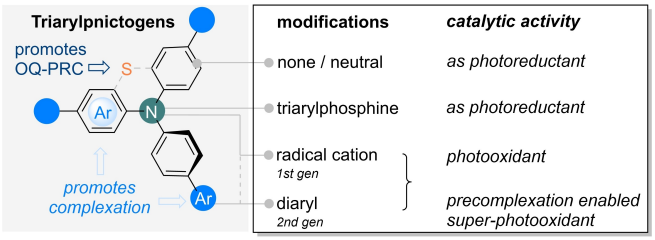

Figure 41. Triarylpnictogen organophotocatalyst core structure, reported modification strategies and their photocatalytic reactivities.

shell photocatalysis. The heterocyclic phenothiazine derivatives were shown to merge separate radical polar catalytic cycles into one and computationally the enhancement of precomplexation can be shown by *via* synergistic π–π and S-Li$^+$ interactions.

2.4.1. Triarylamines and phenothiazines as neutral state photoreductants

Considering that triarylamines are electron-rich molecules, it is intuitive that they can act as photoreductants. The HOMO is delocalized over the whole molecule (both on the aryl and N) and LUMO delocalized only on the aryl ring.[94] Hammett correlations with redox properties of triarylamines were observed[95] and dimerization of radical cation at the *para*-position of their aryl groups were reported.[94] Thus, electron-withdrawing or electron-donating groups are often added at the *para*- positions to tune photoredox properties or prevent catalyst decomposition.[67,96] One of the most recent examples of triarylamines as reducing Org**PC**s leverages strong EDA interactions (Figure 42).

Procter and co-workers demonstrated a photocatalytic C–H functionalization of arenes featuring the *in situ* generation of triaryl sulfonium salts (as redox handles)[97] such as **25 a** or **25 b** *via* an interrupted Pummerer reaction (Figure 42).[98] This is achieved by photoreduction of **25 a** or **25 b** by Org**PC 26 a** or **26 b** respectively. Both Org**PC** – substrate combinations show EDA complex formation. The design of **26 a** and **26 b** featured the presence of halogen, presumably to tune the redox properties, while **26 a** also contained a napthalene core to enhance non-covalent interactions. Org**PC 25** was used for C–H alkylations while **26** was used for C–H cyanation reactions.

N-aryl phenothiazines (**PTH**) are sulfur-containing amine heterocycles which are also used as photocatalysts.[99] The enhanced reducing capability is perhaps brought about by the radical cation stabilization brought by the sulfur atom. In a series of studies, Nagao and co-workers merged PRC with radical polar crossover (RPC) chemistry using a single catalyst whose design was based on **PTH** (Figure 43). The inspiration came from the dual [Ru] (as photocatalyst) and sulfur-containing tetrathiafulvalene (TTF, as a RPC catalyst) system of Murphy and co-workers (Figure 43B).[101] In the SAR studies of Nagao and co-workers, they found out that both the S atom (for RPC) and the naphthyl- moiety (for substrate preassembly) are

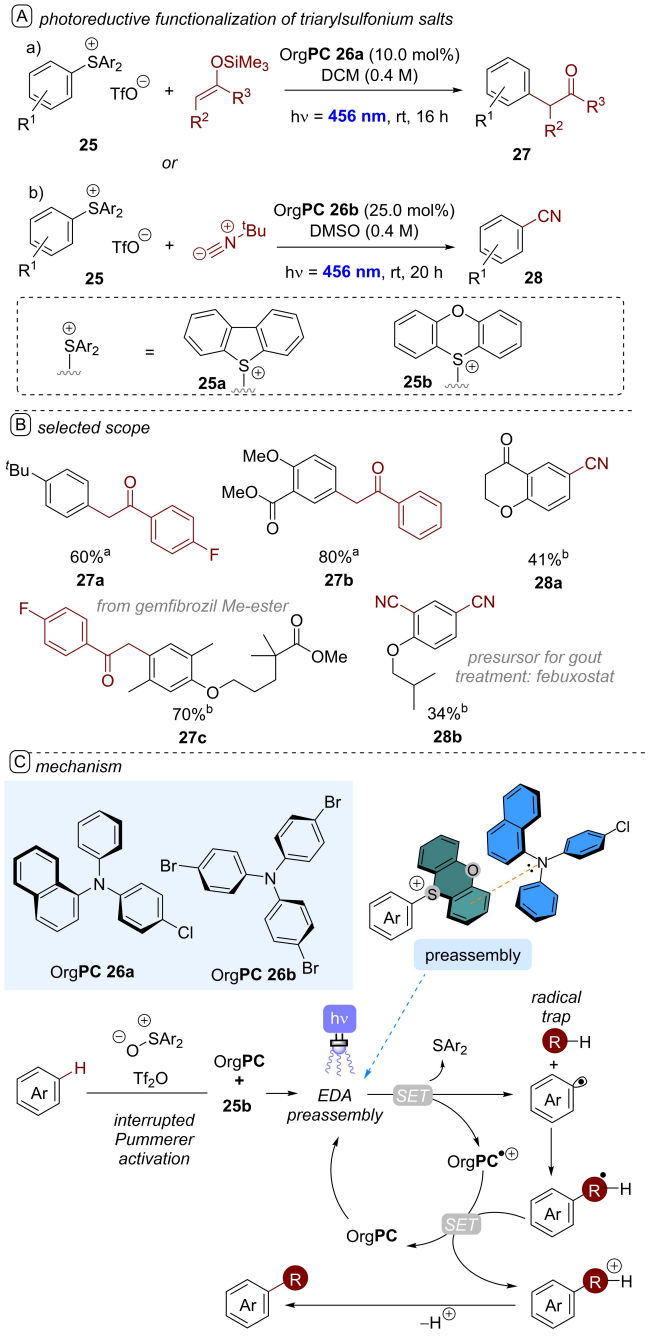

Figure 42. A) Triarylamines as organophotoreducing catalysts used for alkylation and cyanation of triarylsulfonium salts. B) selected scope. C) mechanism *via* excitation of an EDA complex.

needed for optimum catalyst performance and identified **PTH-1** and **PHT-2** as the optimum Org**PC**s. They used these catalysts for decarboxylative couplings of **29** with various nucleophiles such as C(sp^3)–O bond formations, semi-Pinacol rearrangements, *N*-alkylations of sulfonamides, and three component couplings *with* alcohols and styrenes (Figure 44).[102] Key to reactivity was the strong EDA complex observed between the catalyst and target substrate. Noticing the key requirements for the catalyst's naphthyl group, S atom and the reaction's Li

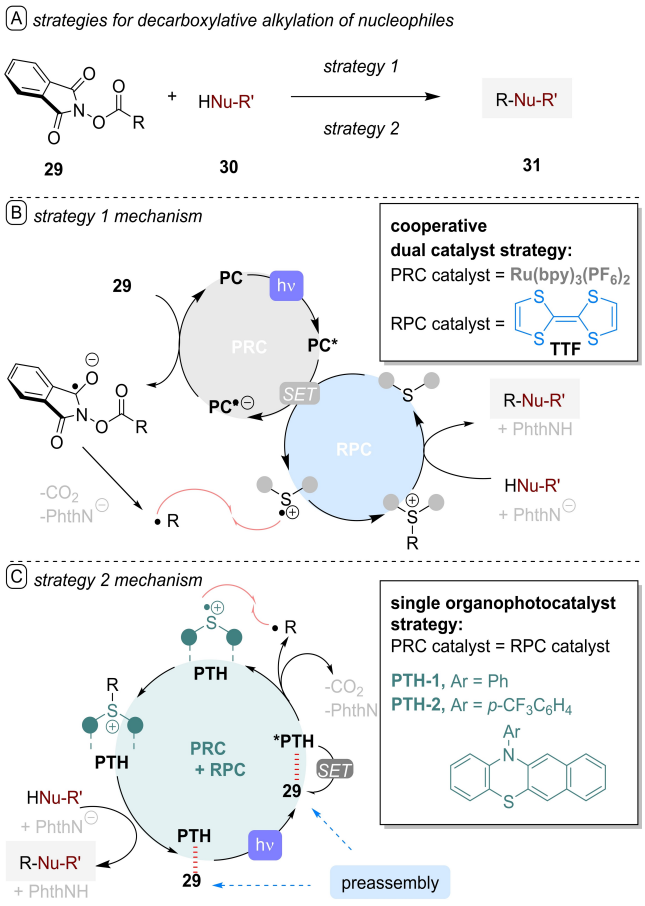

Figure 43. A) decarboxylative functionalization reaction using B) [Ru] and TTF catalyst system or C) **PTH** as 2-in-1 PRC and RPC catalyst.

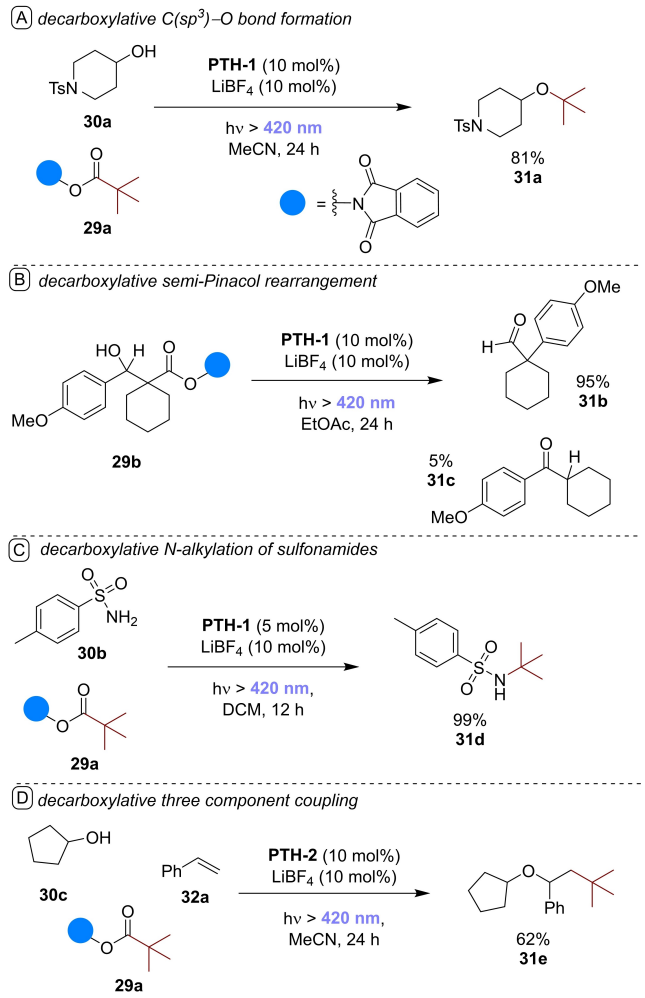

Figure 44. PTH as a 2-in-1 PRC and RPC catalyst for different reactions.

additive, computation of a possible mode of substrate–catalyst preassembly identified a highly favorable (exergonic) synergistic π–π interaction and an interaction between the S atom and Li cation as a weak Lewis acid (Figure 45).

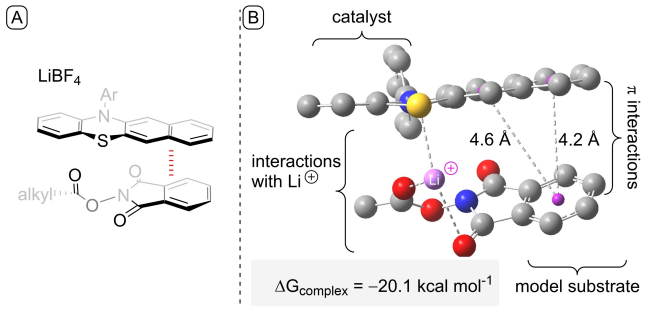

Figure 45. A) Proposed interaction by Nagao, Ohmiya and co-workers. B) Computational investigation for complexation of Org**PC** with a model substrate. Calculated using ωB97XD / 6–31 + + g(d,p) level of theory. Centroid-to-centroid distances were defined as from the centroids of the substrate's benzene ring to the centroids of each individual benzene rings of the catalyst's naphthalene fragment. Color legends: grey = C, red = O, blue = N, yellow = S, pink = Li, magenta = centroid, H atoms and BF_4^- are removed for clarity.

Another recent strategy used for triarylamine photocatalyst design leverages halogen bonding with the substrate.[103,104] Nanjo, Takemoto and co-workers appended pyridine (**33**) as the halogen bond donor for the reduction of alkyl bromides such as **34** (Figure 46).[104] Upon interception of the generated radical by traps such as **35**, oxidation and deprotonation generates the product **36** and closes the catalytic cycle. We note that there are other examples in recent literature where halogen bonds between tertiary amine derivatives and aryl halides are exploited in photocatalysis.[103]

2.4.2. Triarylphosphine-NaI as neutral state photoreductants

The importance of cation-π interactions for transition state stabilization are well-established in catalysis.[105] This was further demonstrated in photocatalysis when Shang, Fu and co-workers introduced the use of PPh_3 (catalyst) and NaI (sacrificial reductant) for a photocatalytic decarboxylative arylation (and alkylation) reaction (Figure 47).[106a] Using DFT calculations, they discovered that the substrate **29c**, NaI, and PPh_3 form a

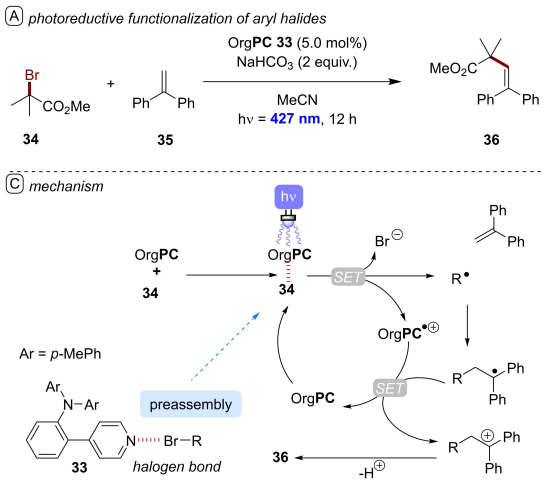

Figure 46. A) Halogen bond-assisted reductive activation of alkyl bromides using a triarylamine photocatalyst. B) mechanism.

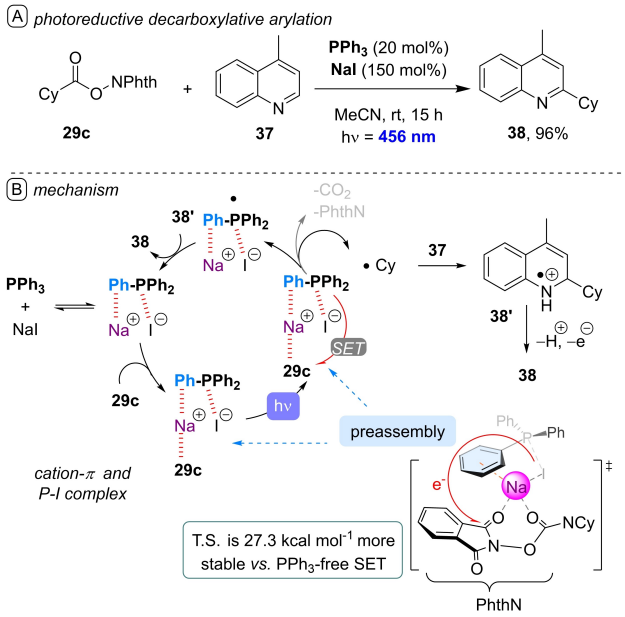

Figure 47. A) **TPP**/NaI complex as a reductive photocatalyst used for a decarboxylative arylation reaction B) Proposed mechanism.

favorable three-component precomplex. It features both cation-π and P–I non-covalent interactions. Moreover, they found out that PPh_3 plays an important role in the precomplex as the activation energy for SET of this complex is 27.3 $kcal^{-1}$ lower than PPh_3-free SET.

2.4.3. Triarylamines and phenothiazines as oxidized state 'super' photooxidants

As shown by Wasielewski and co-workers[106b] for phenothiazine radical cations and later by Barham & co-workers for acyclic tri-*p*-substituted arylaminium radical cations[67] (**TPA**$^{\bullet+}$s), radical cationic photocatalysts have ultrashort lifetimes (on the pico-second domain, e.g. <10 ps for **TPA**$^{\bullet+}$s and **PTZ**$^{\bullet+}$s), thus bimolecular quenching by diffusion control is not feasible. However, radical cationic photocatalysts nonetheless deliver productive synthetic photochemistry, as demonstrated by several independent groups.[54] By changes in the ground-state UV-vis and EPR spectra of **TPA**$^{\bullet+}$s, Barham and co-workers demonstrated for the first time a non-covalent assembly between a radical ion photocatalyst and target substrate prior to photoexcitation,[67] and subsequently together with the Hauer group confirmed how this allows to harness excited doublet states in photocatalysis.[68] In this case, an aryl chloride such as **8a'** assembling at the biaryl 'propellor' of the **TPA**$^{\bullet+}$ (specifically, at a T–π (or edge-to-face) orientation) allows excited-state SET to occur effectively in 'pseudo-intramolecular' fashion (Figure 48). Note that π–π (face-to-face) precomplexation is still operative, and is the favored mode for the synthetically unreactive/less reactive substrates. However, this is unreactive either i) because it is less accessible (steric repulsive term dominates) or ii) because it encourages the **TPA**$^{\bullet+}$ to adopt a conformation in which hole density (oxidizing power) is delocalized. The radical is then intercepted by a nitrogen heterocycle such as **39** forming the C–N coupling product **40**. A similar reaction was reported by Wickens and co-workers but with **PTH**$^{\bullet+}$ and moderately electron-rich alkylarenes or more challenging benzene, whereby this time the reaction perhaps benefitted from a very high concentration (excess) of arene. In this case, without an 'organized' preassembly, there is statistically likely to be an arene molecule in close enough proximity

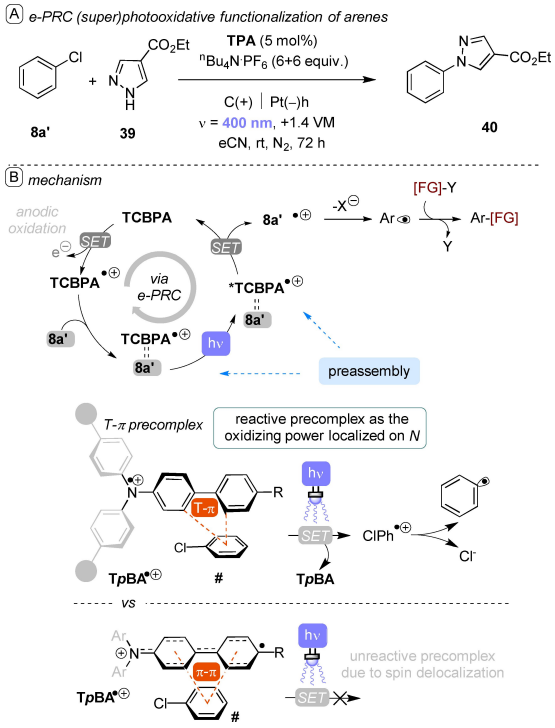

Figure 48. A) **TPA**$^{\bullet+}$ as a (super) oxidative organophotocatalyst for oxidative arylation of nitrogen heterocycles. B) mechanism and productive *vs.* unproductive modes of preassembly.

to the excited state as it is generated to enable the reaction by static quenching, *vide supra*.

2.5. Acridinium salts

Seminal reports of Fukuzumi and co-workers[107] on the development and characterization of photophysical properties of 9-mesityl-10-methylacridinium ion (Mes-Acr$^+$) popularized the use of these salts as organophotocatalysts for challenging SET oxidations. Acridinium-based photocatalysts typically comprise a linked donor-acceptor moieties, whereby mesitylene (Mes) is an electron donor and 10-alkyl/aryl acridinium cation (Acr$^+$) is an electron acceptor (Figure 49).[108,109] They exhibit long-lasting CT-state lifetimes with broad redox windows that are pH independent. The improvements in chemical stability and photophysical properties of these catalysts is greatly owed to extensive historical efforts assessing various amendments to the core. Fukuzumi initially overcame photobleaching of these catalysts by introducing a sterically demanding mesityl group at the C9 position. Further efforts to improve chemical stability involved using an *N*-aryl instead of an *N*-alkyl substituent. Typically, acridinium salts can be prepared from an acridone with organometallic nucleophilic addition to give a tertiary alcohol which undergoes dehydration after protonation to yield desired acridinium core (Figure 50A).[110] Alternatively, acridinium salts can be accessed by a one-step synthesis of tetrasubstituted acridinium core *via* a Friedel–Crafts reaction using triarylamines and benzoyl chloride derivatives (Figure 50B).[108,109]

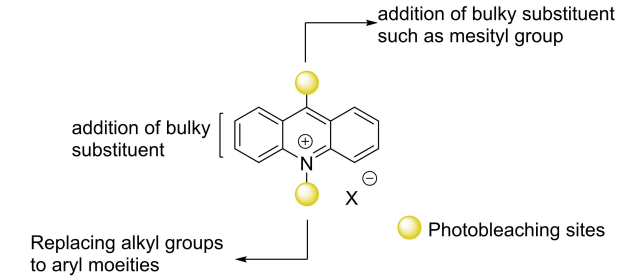

Figure 49. Acridinium salts core structure and sites for modifications.

Acridinium salts have been effectively used as photooxidative catalysts for various substrates, such as the oxidation of alkenes and arenes[110] which has been previously reviewed.[108,109] A photoinduced charge-transfer state gives rise to an intramolecular electron transfer from the mesityl to the acridinium groups to access *[**Mes-Acr**$^+$] (Acr$^\bullet$-Mes$^{\bullet+}$) which has high oxidative power ($^*E_{1/2} = +2.18$ V). The orthogonal arrangement of mesityl and acridinium moieties prevents charge recombination, resulting in a longer excited-state lifetime. *[**Mes-Acr**$^+$] can then oxidize substrates (Figure 51).

2.5.1. Acridinium salts as photooxidants

Though high oxidation potential of acridinium salts is beneficial to achieve challenging oxidations, it also poses risks of unselective oxidation. Nicewicz, DiRocco and co-workers[111] overcame the issues of unselective oxidation (lower product yields), by introducing different substituents – mostly electron-donating moieties – at the 1,3,5,6-positions of acridinium salts in order to decrease excited state oxidative redox power. Catalytic performances of different analogues of acridinium salts are shown *via* the decarboxylative conjugate addition of Cbz-proline to dimethyl maleate (Figure 52). 9-mesityl-10-methylacridinium **43a** ($^*E_{1/2} = +2.06$ V) gives only a 5% yield of **42** compared to electron-rich acridinium salts **43e** ($^*E_{1/2} = +1.65$ V) and **43f** ($^*E_{1/2} = +1.62$ V). There are of course numerous examples of catalytic photooxidative transformations using acridinium salt photocatalysts, but this example clearly shows how structural and electronic modification of acridinium salt catalysts helped to achieve higher product yields.

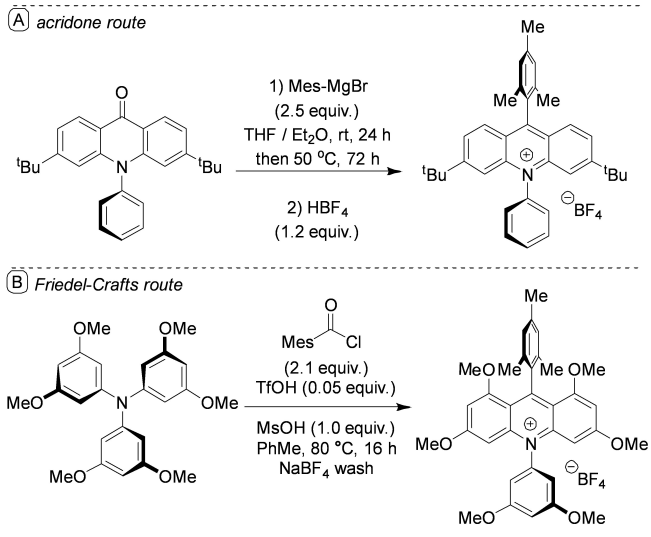

Figure 50. Representative synthesis of acridinium salts.

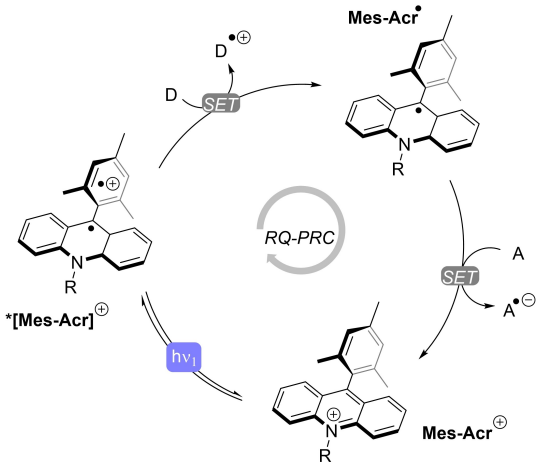

Figure 51. Photooxidation mechanism of **Mes-Acr**$^+$.

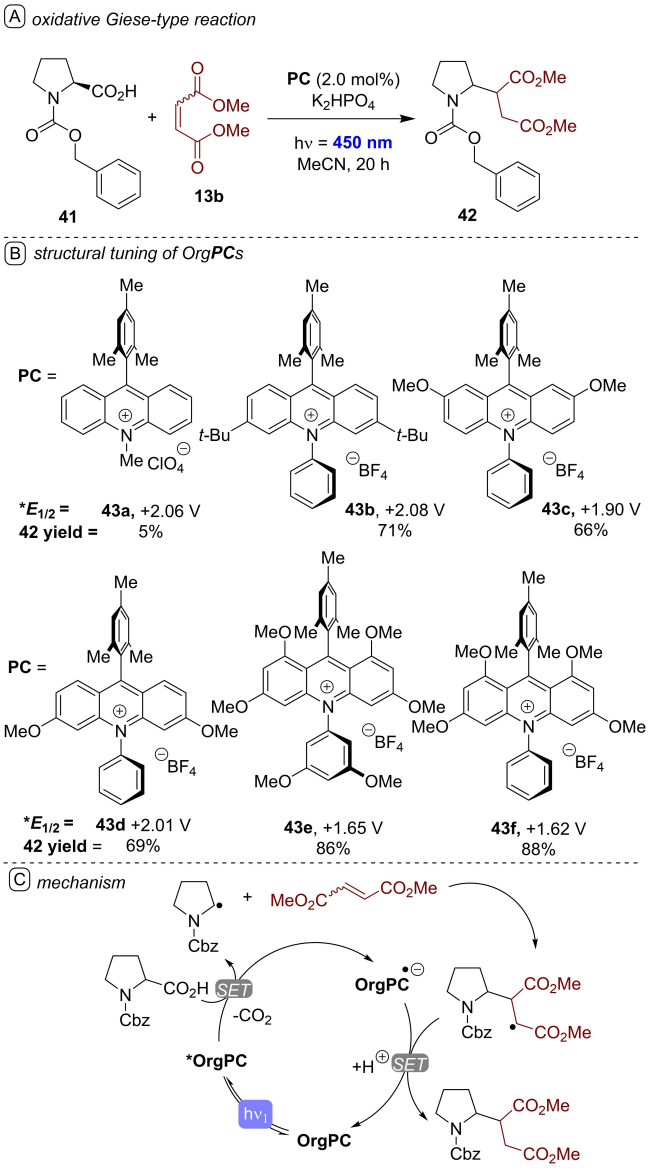

Figure 52. Oxidative Giese-type reaction catalyzed by OrgPC = **Mes-Acr**$^+$. Potentials *vs.* SCE.

2.5.2. Mes-Acr$^+$-derived acridine radical as a super photoreductant

In contrast to the well-established photooxidation properties of acridinium salts, recently, Nicewicz and co-workers reported the generation of acridine radicals from acridinium salts, the former serving as super photoreductants *via* a conPET cycle.[112] They showed that the maximum $*E^0$ of the neutral acridine radical is as low as −3.36 V which makes it one of the most potent photoreductants ever reported, on par with dissolving alkali metal reducing conditions. Computational and spectroscopic analysis revealed that non-planar dihedral angle (36°) between the acridinium core and the *N*-phenyl fragment – a twisted intramolecular charge-transfer (TICT) state – is responsible for a high energy charge transfer state. Experimentally, this charge transfer state is corroborated by an observed debromination when brominated acridinium was subjected to reaction conditions. This super reducing photoexcited acridine radical boasted applications in chemoselective dehalogenation and detosylation reactions (Figure 53).[112]

2.6. Other selected organophotocatalyst scaffolds

As mentioned in section 1.3, this review was not designed to be comprehensive in covering all Org**PC** families and their structural modifications. Two other families of Org**PC**s are now briefly presented. Although neither access particularly high redox potentials nor include evidence to suggest non-covalent assemblies, the following classes of Org**PC**s do have a broad redox window and can be viewed as replacements for transition metal-based photocatalysts.

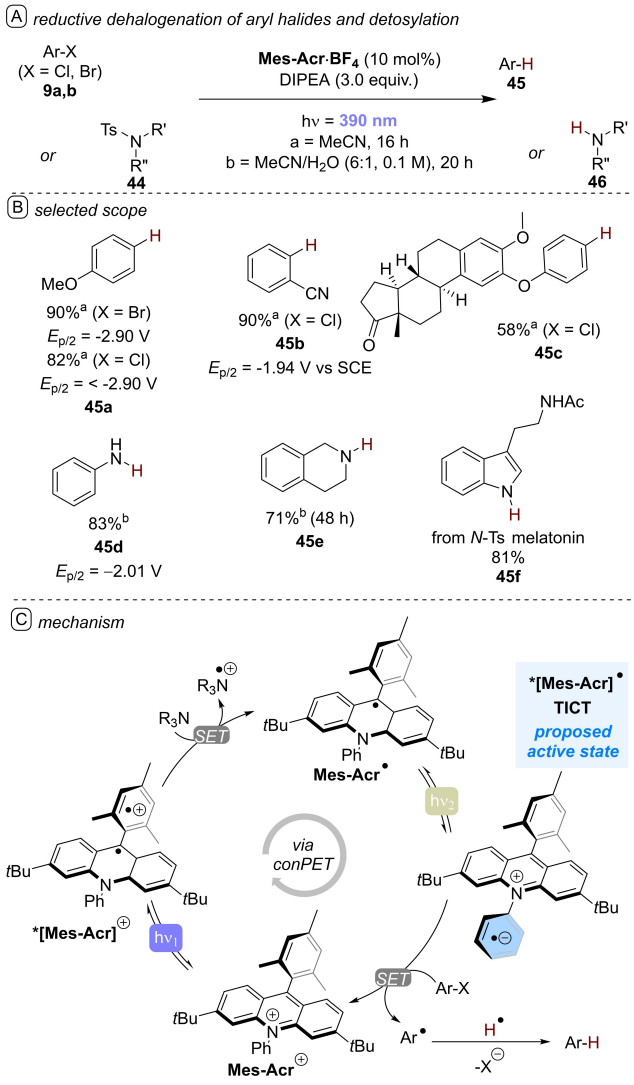

Figure 53. Mes-Acr$^+$-derived acridine radical as a (super) photoreductant *via* a conPET mechanism. Potentials *vs.* SCE.

2.6.1. DPZ as neutral state photooxidants

Bureš, Jiang and co-workers developed 4,5-disubstituted pyrazine-2,3-dicarbonitrile (**DPZ**) which is another organophotocatalyst with spatially separated donor-acceptor fragments operating *via* a RQ-PRC pathway (Figure 54).[113] The LUMO is situated at the heterocyclic pyrazine core, while the HOMO is at the electron rich heteroaromatic fragment. Structural modifications at the heteroaromatic fragment allows tuning of its redox and photophysical properties. A recent application of this photocatalyst is a formal and enantioconvergent radical substitution with chiral phosphoric acid (**CPA**) as co-catalyst affording **48** from alkyl halide **46** and amino acid **47**.[114]

2.6.2. Naphthochromenone photocatalysts

Dell'Amico and coworkers introduced naphthochromenones (**NTC**) which exhibit both oxidative and reductive properties. Synthesis of the **NTC** core is achieved in two steps (Figure 55). The first involves photo-[4+2] cycloaddition of benzophenone **49** and coumarin **50** to form the tetracyclic product **51** (under flow conditions). Then, acid-catalyzed dehydration of **51** and subsequent aromatization yields the desired **NTC**.[115]

NTCs are another class of organophotocatalysts whereby photoredox properties can be altered by structural modifications (Figure 56).[115] TD-DFT calculations showed that the HOMO, LUMO and LUMO+1 are all localized on the **NTC**'s core. The replacement of a phenyl group at position 7 with H resulted in a hypsochromic shift (10 nm) in the UV-vis absorption and a longer excited state lifetime. More interestingly, modifications at position 3 have more pronounced effects on the photoredox properties of NTC. Adding electron donating groups or extending the conjugation at position 3 enhances the photoreducing properties of **NTC** (with *E* ($PC^{\bullet+}$/PC*) reaching up to −1.77 V *vs.* SCE). On the other hand, electron-withdrawing groups at position 3 gave positive *E* ($PC^{\bullet-}$/PC*) values of up to +1.65 V *vs.* SCE. With this broad redox window, **NTC**s were able to participate effectively in oxidative or reductive quenching manifolds (e.g. reactions involving decarboxylation, desilylation, and dehalogenations).

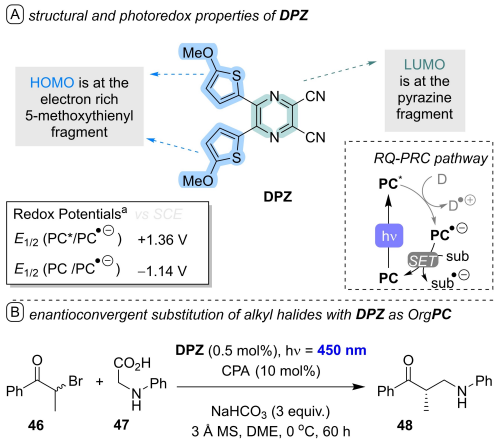

Figure 54. A) **DPZ** as organophotocatalyst. [a] in MeCN . B) Recent application.

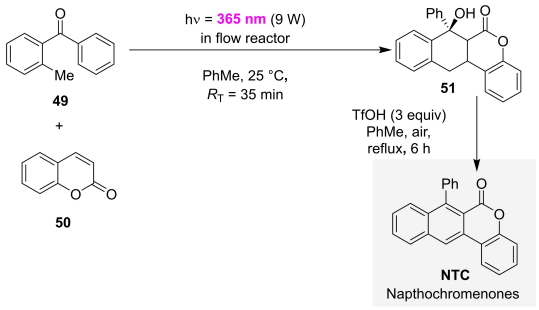

Figure 55. Synthesis of napthochromenone (**NTC**) catalysts.

3. Summary and Conclusion

In this review, five organophotocatalyst cores were evaluated which can be programmed to divert photochemical reaction mechanisms. The effect of and leveraging on structural modification, redox states, preassemblies, and aggregation states was discussed. Bulky groups or sidechains affects the kinetics of SET by: i) preventing unwanted interactions; ii) increasing the reorganization energy of the system. The possibility of slowing down SET by pushing it towards the Marcus inverted region (i.e. too exergonic) should not be discounted. The presence of non-covalent interactions are beneficial especially for short-lived excited state as: i) they allow to circumvent the diffusion barrier; ii) decrease the distance between reacting species; and iii) lower the activation energy of SET. In this review we have seen modes of these preassemblies assisted by π–π, cation-π, and halogen bonding interactions. Computational investigations were carried out for some assemblies. We hope to encourage researchers to probe deeper on their mechanistic investigation and instill an informed line of thinking (based on the patterns uncovered above) when setting-up a reaction or designing new catalysts in the future. We envisage exciting opportunities in targeted organophotocatalyst modifications to influence aggregation states and excited state mechanisms, that together with advances in solvent-influenced aggregation/microstructuring[116] will unlock a new paradigm of selective synthetic photocatalytic processes.

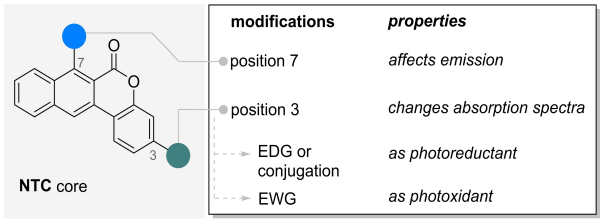

Figure 56. NTC organophotocatalyst core structure, modification and photocatalytic reactivities.

Acknowledgements

M. J. P. M. is grateful for funding provided by the SynCat programme of the Elite Network of Bavaria as a Master student at the University of Regensburg and is now a Ph.D. student within the ESPRC Centre of Doctoral Training 'Technology Enhanced Chemical Synthesis' at the University of Bristol. J. K. and J. P. B. are members of DFG TRR 325 'Assembly Controlled Chemical Photocatalysis' (444632635) and thank other members of the TRR for insightful discussions. J. K. and J. P. B. acknowledge funding provided by the Alexander von Humboldt Foundation within the framework of the Sofja Kovalevskaja Award endowed by the German Federal Ministry of Education and Research. Open Access funding enabled and organized by Projekt DEAL.

Conflict of Interest

The authors declare no conflict of interest.

Data Availability Statement

The data that support the findings of this study are available in the supplementary material of this article.

Keywords: organophotocatalysis · mechanistic switchover · Marcus theory · anti-Kasha photochemistry · non-covalent assemblies

[1] H. E. Bonfield, T. Knauber, F. Lévesque, E. G. Moschetta, F. Susanne, L. J. Edwards, *Nat. Commun.* **2020**, *11*, 804.
[2] a) G. Ciamician, *Science* **1912**, *36*, 385–394; b) A. Eibner, *Chem.-Ztg.* **1911**, *35*, 753–755; c) B. König, *Eur. J. Org. Chem.* **2017**, *2017*, 1979–1981.
[3] a) At the time of writing this review, a google scholar search for "photocatalysis" from the year 2000 to 2022 gave 284, 000 results; b) L. Marzo, S. K. Pagire, O. Reiser, B. König, *Angew. Chem., Int. Ed.* **2018**, *57*, 10034–10072; *Angew. Chem.* **2018**, *130*, 10188–10228; c) M. Melchionna, P. Fornasiero, *ACS Catal.* **2020**, *10*, 5493–5501; d) M. H. Shaw, J. Twilton, D. W. C. MacMillan, *J. Org. Chem.* **2016**, *81*, 6898–6926.
[4] a) L. Candish, K. D. Collins, G. C. Cook, J. J. Douglas, A. Gómez-Suárez, A. Jolit, S. Keess, *Chem. Rev.* **2022**, *122*, 2907–2980; b) G. E. M. Crisenza, P. Melchiorre, *Nat. Commun.* **2020**, *11*, 803; c) P. Li, J. A. Terrett, J. R. Zbieg, *ACS Med. Chem. Lett.* **2020**, *11*, 2120–2130; d) D. Petzold, M. Giedyk, A. Chatterjee, B. König, *Eur. J. Org. Chem.* **2020**, *2020*, 1193–1244; e) S. Reischauer, B. Pieber, *iScience* **2021**, *24*, 102209.
[5] a) C. R. J. Stephenson, T. P. Yoon, D. W. C. MacMillan (Eds.) *Visible Light Photocatalysis in Organic Chemistry*, 1st ed., Wiley-VCH Verlag GmbH & Co. KGaA, Weinheim, **2018**; b) C. K. Prier, D. A. Rankic, D. W. C. MacMillan, *Chem. Rev.* **2013**, *113*, 5322–5363.
[6] S. G. E. Amos, M. Garreau, L. Buzzetti, J. Waser, *Beilstein J. Org. Chem.* **2020**, *16*, 1163–1187.
[7] D. A. Nicewicz, T. M. Nguyen, *ACS Catal.* **2014**, *4*, 355–360.
[8] S. P. Pitre, C. D. McTiernan, J. C. Scaiano, *ACS Omega* **2016**, *1*, 66–76.
[9] N. A. Romero, D. A. Nicewicz, *Chem. Rev.* **2016**, *116*, 10075–10166.
[10] M. K. Bogdos, E. Pinard, J. A. Murphy, *Beilstein J. Org. Chem.* **2018**, *14*, 2035–2064.
[11] A. Vega-Peñaloza, J. Mateos, X. Companyó, M. Escudero-Casao, L. Dell'Amico, *Angew. Chem., Int. Ed.* **2021**, *60*, 1082–1097; *Angew. Chem.* **2021**, *133*, 1096–1111.
[12] W. Yao, E. A. Bazan-Bergamino, M.-Y. Ngai, *ChemCatChem* **2022**, *14*, e202101292.
[13] T. Förster, *Ann. Phys.* **1948**, *437*, 55–75.
[14] D. L. Dexter, *J. Chem. Phys.* **1953**, *21*, 836–850.
[15] For a recent review about Energy transfer photocatalysis, see: F. Strieth-Kalthoff, M. J. James, M. Teders, L. Pitzer, F. Glorius, *Chem. Soc. Rev.* **2018**, *47*, 7190–7202.
[16] G. Masson, B. König, *Eur. J. Org. Chem.* **2020**, *2020*, 1191–1192.
[17] T. Noël, E. Zysman-Colman, *Chem Catal.* **2022**, *2*, 468–476.
[18] S. J. Chalk in *The IUPAC Compendium of Chemical Terminology* (Ed.: V. Gold), International Union of Pure and Applied Chemistry (IUPAC), Research Triangle Park, NC, **2019**.
[19] In simple terms, spectral overlap is the area where the normalized emission spectrum of the donor overlaps with the normalized absorption spectrum of the acceptor. Practically speaking, the greater the overlap, the greater the number of EnT events. This can be approximated by the difference between the Triplet excited energies of the donor and acceptor species.
[20] a) A. Bhattacharyya, S. De Sarkar, A. Das, *ACS Catal.* **2021**, *11*, 710–733; b) D. Bialas, E. Kirchner, M. I. S. Röhr, F. Würthner, *J. Am. Chem. Soc.* **2021**, *143*, 4500–4518.
[21] J. S. Beckwith, A. Aster, E. Vauthey, *Phys. Chem. Chem. Phys.* **2021**, *24*, 568–577.
[22] a) M. Marchini, A. Gualandi, L. Mengozzi, P. Franchi, M. Lucarini, P. G. Cozzi, V. Balzani, P. Ceroni, *Phys. Chem. Chem. Phys.* **2018**, *20*, 8071–8076; b) A. J. Rieth, M. I. Gonzalez, B. Kudisch, M. Nava, D. G. Nocera, *J. Am. Chem. Soc.* **2021**, *143*, 14352–14359.
[23] D. Y. Jeong, D. S. Lee, H. L. Lee, S. Nah, J. Y. Lee, E. J. Cho, Y. You, *ACS Catal.* **2022**, *12*, 6047–6059.
[24] M. Schmalzbauer, M. Marcon, B. König, *Angew. Chem., Int. Ed.* **2021**, *60*, 6270–6292; *Angew. Chem.* **2021**, *133*, 6338–6363.
[25] M. A. Bryden, E. Zysman-Colman, *Chem. Soc. Rev.* **2021**, *50*, 7587–7680.
[26] a) G. E. M. Crisenza, D. Mazzarella, P. Melchiorre, *J. Am. Chem. Soc.* **2020**, *142*, 5461–5476; b) H. Li, Y. Liu, S. Chiba, *JACS Au* **2021**, *1*, 2121–2129; c) Y. Q. Yuan, S. Majumder, M.-H. Yang, S.-R. Guo, *Tetrahedron Lett.* **2020**, *61*, 151506.
[27] for a representative synthesis of 9,10-dibromoanthracene, See: S. Jones, J. C. C. Atherton, *Synth. Commun.* **2001**, *31*, 1799–1802.
[28] a) F. Glöcklhofer, M. Lunzer, J. Fröhlich, *Synlett* **2015**, *26*, 950–952; b) J.-R. Li, Y. Tao, Q. Yu, X.-H. Bu, *Chem. Commun.* **2007**, 1527–1529.
[29] M. J. P. Mandigma, J. Žurauskas, C. I. MacGregor, L. J. Edwards, A. Shahin, L. d'Heureuse, P. Yip, D. J. S. Birch, T. Gruber, J. Heilmann, M. P. John, J. P. Barham, *Chem. Sci.* **2022**, *13*, 1912–1924.
[30] A. P. Schaap, K. A. Zaklika, B. Kaskar, L. W.-M. Fung, *J. Am. Chem. Soc.* **1980**, *102*, 389–391.
[31] Axel G. Griesbeck, Angelika Eske in *Encyclopedia of Reagents for Organic Synthesis*, John Wiley & Sons, Ltd, **2018**.
[32] a) Q.-Q. Zhao, J. Rehbein, O. Reiser, *Green Chem.* **2022**, *24*, 2772–2776; b) Uphill catalysis refers to a pathway that enables chemical transformations *via* high energy open-shell intermediates, that are hard to achieve thermally with closed-shell intermediates. For other photocatalytic examples, see: J. I. Day, K. Singh, W. Trinh, J. D. Weaver, *J. Am. Chem. Soc.* **2018**, *140*, 9934–9941.
[33] a) N. Arai, K. Tanaka, T. Ohkuma, *Tetrahedron Lett.* **2010**, *51*, 1273–1275; b) C. R. Jones, B. J. Allman, A. Mooring, B. Spahic, *J. Am. Chem. Soc.* **1983**, *105*, 652–654.
[34] A. G. Griesbeck, O. Sadlek, K. Polborn, *Liebigs Ann./Recl.* **1996**, *1996*, 545–549.
[35] a) M. A. Cismesia, T. P. Yoon, *Chem. Sci.* **2015**, *6*, 5426–5434; b) S. Lin, M. A. Ischay, C. G. Fry, T. P. Yoon, *J. Am. Chem. Soc.* **2011**, *133*, 19350–19353; c) Y. Yamaguchi, Y. Okada, K. Chiba, *Electrochemistry* **2013**, *81*, 331–333.
[36] P. Clawson, P. M. Lunn, D. A. Whiting, *J. Chem. Soc. Perkin Trans. 1* **1990**, 153–157.
[37] a) E. Alfonzo, A. B. Beeler, *Chem. Sci.* **2019**, *10*, 7746–7754; b) E. Alfonzo, F. S. Alfonso, A. B. Beeler, *Org. Lett.* **2017**, *19*, 2989–2992.
[38] We recognize the limitation of DFT in describing charge transfer character and thus our calculation might be underestimating the actual interactions between the catalyst and substrate. Nevertheless, the more exergonic complexation of **DCA** vs **DTAC** and the geometric arguments are deemed sufficient computational agreements with the experimental observation of Beeler and co-workers.
[39] S. Fukuzumi, K. Ohkubo, T. Suenobu, K. Kato, M. Fujitsuka, O. Ito, *J. Am. Chem. Soc.* **2001**, *123*, 8459–8467.
[40] For a recent review about the effect of reaction conditions on photocatalysis, see Y. Sakakibara, K. Murakami, *ACS Catal.* **2022**, *12*, 1857–1878. For an important example, see: T. D. Svejstrup, A.

Chatterjee, D. Schekin, T. Wagner, J. Zach, M. J. Johansson, G. Bergonzini, B. König, *ChemPhotoChem* **2021**, *5*, 808–814.
[41] a) S. M. Bonesi, M. Fagnoni, A. Albini, *Eur. J. Org. Chem.* **2008**, *2008*, 2612–2620; b) S. M. Bonesi, I. Manet, M. Freccero, M. Fagnoni, A. Albini, *Chem.-Eur. J.* **2006**, *12*, 4844–4857; c) A. F. Olea, D. R. Worrall, F. Wilkinson, S. L. Williams, A. A. Abdel-Shafi, *Phys. Chem. Chem. Phys.* **2002**, *4*, 161–167; d) T. Sakurai, Y. Uematsu, O. Tanaka, H. Inoue, *J. Chem. Soc. Perkin Trans. 2* **1992**, 2163–2167.
[42] E. Baciocchi, T. Del Giacco, F. Elisei, M. F. Gerini, M. Guerra, A. Lapi, P. Liberali, *J. Am. Chem. Soc.* **2003**, *125*, 16444–16454.
[43] For a recent discussion on the effect of solvents in photocatalysis See: R. K. Venkatraman, A. J. Orr-Ewing, *Acc. Chem. Res.* **2021**, *54*, 4383–4394.
[44] a) J. D. Earley, A. Zieleniewska, H. H. Ripberger, N. Y. Shin, M. S. Lazorski, Z. J. Mast, H. J. Sayre, J. K. McCusker, G. D. Scholes, R. R. Knowles, O. G. Reid, G. Rumbles, *Nat. Chem.* **2022**, *14*, 746–753; b) For a study exploring the role of counterions in photocatalysis, see: E. P. Farney, S. J. Chapman, W. B. Swords, M. D. Torelli, R. J. Hamers, T. P. Yoon, *J. Am. Chem. Soc.* **2019**, *141*, 6385–6391.
[45] J. Eriksen, C. S. Foote, *J. Am. Chem. Soc.* **1980**, *102*, 6083–6088.
[46] R. C. Kanner, C. S. Foote, *J. Am. Chem. Soc.* **1992**, *114*, 678–681.
[47] C. Schweitzer, R. Schmidt, *Chem. Rev.* **2003**, *103*, 1685–1758.
[48] a) J. Santamaria, *Pure Appl. Chem.* **1995**, *67*, 141–147; b) J. Santamaria, R. Ouchabane, J. Rigaudy, *Tetrahedron Lett.* **1989**, *30*, 3977–3980.
[49] a) For related studies, see: J. Santamaria, P. Gabillet, L. Bokobza, *Tetrahedron Lett.* **1984**, *25*, 2139–2142; b) T. B. Truong, J. Santamaria, *J. Chem. Soc. Perkin Trans. 2* **1987**, 1–5.
[50] a) M. F. Acquavella, M. E. Evans, S. W. Farraher, C. J. Nevoret, C. J. Abelt, *J. Org. Chem.* **1994**, *59*, 2894–2897; b) F. Glöcklhofer, A. J. Morawietz, B. Stöger, M. M. Unterlass, J. Fröhlich, *ACS Omega* **2017**, *2*, 1594–1600.
[51] a) T. Hinoue, Y. Shigenoi, M. Sugino, Y. Mizobe, I. Hisaki, M. Miyata, N. Tohnai, *Eur. J. Chem.* **2012**, *18*, 4634–4643; b) Y. Mizobe, T. Hinoue, A. Yamamoto, I. Hisaki, M. Miyata, Y. Hasegawa, N. Tohnai, *Chem. Eur. J.* **2009**, *15*, 8175–8184.
[52] a) S. K. Silverman, C. S. Foote, *J. Am. Chem. Soc.* **1991**, *113*, 7672–7675; b) E. Baciocchi, T. Del Giacco, A. Lapi, *Org. Lett.* **2004**, *6*, 4791–4794.
[53] a) J. Liu, L. Lu, D. Wood, S. Lin, *ACS Cent. Sci.* **2020**, *6*, 1317–1340; b) F. Glaser, C. Kerzig, O. S. Wenger, *Angew. Chem., Int. Ed.* **2020**, *59*, 10266–10284; *Angew. Chem.* **2020**, *132*, 10350–10370.
[54] S. Wu, J. Kaur, T. A. Karl, X. Tian, J. P. Barham, *Angew. Chem., Int. Ed.* **2022**, *61*, e202107811; *Angew. Chem.* **2021**, *134*, e202107811.
[55] J. P. Barham, B. König, *Angew. Chem. Int. Ed.* **2020**, *59*, 11732–11747; *Angew. Chem.* **2020**, *132*, 11828–11844.
[56] M. Neumeier, D. Sampedro, M. Májek, V. A. de la Peña O'Shea, A. Jacobi von Wangelin, R. Pérez-Ruiz, *Chem.-Eur. J.* **2018**, *24*, 105–108.
[57] I. Ghosh, T. Ghosh, J. I. Bardagi, B. König, *Science* **2014**, *346*, 725–728.
[58] H. Kim, H. Kim, T. H. Lambert, S. Lin, *J. Am. Chem. Soc.* **2020**, *142*, 2087–2092.
[59] a) F. Glaser, O. S. Wenger, *JACS Au* **2022**, *2*, 1488–1503; b) F. Glaser, O. S. Wenger, *Chem. Sci.* **2023**, *14*, 149–161.
[60] J. Eriksen, H. Lund, A. I. Nyvad, *Acta Chem. Scand.* **1983**, *37b*, 459–466.
[61] D. T. Breslin, M. A. Fox, *J. Phys. Chem.* **1994**, *98*, 408–411.
[62] M. Fujita, A. Ishida, T. Majima, S. Takamuku, *J. Phys. Chem.* **1996**, *100*, 5382–5387.
[63] C. A. Hunter, J. K. M. Sanders, *J. Am. Chem. Soc.* **1990**, *112*, 5525–5534.
[64] C. Zhang, *J. Comput. Chem.* **2011**, *32*, 152–160.
[65] J. Haimerl, I. Ghosh, B. König, J. Vogelsang, J. M. Lupton, *Chem. Sci.* **2019**, *10*, 681–687.
[66] X. Tian, T. A. Karl, S. Reiter, S. Yakubov, R. de Vivie-Riedle, B. König, J. P. Barham, *Angew. Chem., Int. Ed.* **2021**, *60*, 20817–20825; *Angew. Chem.* **2021**, *133*, 20985–20993.
[67] S. Wu, J. Žurauskas, M. Domański, P. S. Hitzfeld, V. Butera, D. J. Scott, J. Rehbein, A. Kumar, E. Thyrhaug, J. Hauer, J. P. Barham, *Org. Chem. Front.* **2021**, *8*, 1132–1142.
[68] A. Kumar, P. Malecvich, L. Mewes, S. Wu, J. P. Barham, J. Hauer, *J. Chem. Phys.* **2023**, DOI: 10.1063/5.0142225.
[69] a) A. P. Demchenko, V. I. Tomin, P.-T. Chou, *Chem. Rev.* **2017**, *117*, 13353–13381; b) J. P. Cole, D.-F. Chen, M. Kudisch, R. M. Pearson, C.-H. Lim, G. M. Miyake, *J. Am. Chem. Soc.* **2020**, *142*, 13573–13581.
[70] J. Luo, J. Zhang, *ACS Catal.* **2016**, *6*, 873–877.
[71] S. M. Engle, T. R. Kirkner, C. B. Kelly, *Org. Synth.* **2019**, *96*, 455–473.
[72] H. Uoyama, K. Goushi, K. Shizu, H. Nomura, C. Adachi, *Nature* **2012**, *492*, 234–238.
[73] a) T.-Y. Shang, L.-H. Lu, Z. Cao, Y. Liu, W.-M. He, B. Yu, *Chem. Commun.* **2019**, *55*, 5408–5419; b) P. P. Singh, V. Srivastava, *Org. Biomol. Chem.* **2021**, *19*, 313–321.
[74] C. P. Chernowsky, A. F. Chmiel, Z. K. Wickens, *Angew. Chem. Int. Ed.* **2021**, *60*, 21418–21425; *Angew. Chem.* **2021**, *133*, 21588–21595.
[75] J. Xu, J. Cao, X. Wu, H. Wang, X. Yang, X. Tang, R. W. Toh, R. Zhou, E. K. L. Yeow, J. Wu, *J. Am. Chem. Soc.* **2021**, *143*, 13266–13273.
[76] a) E. Speckmeier, T. G. Fischer, K. Zeitler, *J. Am. Chem. Soc.* **2018**, *140*, 15353–15365.b) M. Streiter, T. G. Fischer, C. Wiebeler, S. Reichert, J. Langenickel, K. Zeitler, C. Deibel, *J. Phys. Chem. C.* **2020**, *124*, 15007–15014.
[77] F. Le Vaillant, M. Garreau, S. Nicolai, G. Gryn'ova, C. Corminboeuf, J. Waser, *Chem. Sci.* **2018**, *9*, 5883–5889.
[78] Y. Liu, X.-L. Chen, X.-Y. Li, S.-S. Zhu, S.-J. Li, Y. Song, L.-B. Qu, B. Yu, *J. Am. Chem. Soc.* **2021**, *143*, 964–972.
[79] S. Grotjahn, B. König, *Org. Lett.* **2021**, *23*, 3146–3150.
[80] A. F. Chmiel, O. P. Williams, C. P. Chernowsky, C. S. Yeung, Z. K. Wickens, *J. Am. Chem. Soc.* **2021**, *143*, 10882–10889.
[81] A. R. Flynn, K. A. McDaniel, M. E. Hughes, D. B. Vogt, N. T. Jui, *J. Am. Chem. Soc.* **2020**, *142*, 9163–9168.
[82] T. Bortolato, M. Dyguda, A. Vega-Peñaloza, L. Dell'Amico, *Synthesis* **2022**, *54*, 3409–3413.
[83] a) F. Würthner, *Chem. Commun.* **2004**, 1564–1579; b) N. T. La Porte, J. F. Martinez, S. Chaudhuri, S. Hedström, V. S. Batista, M. R. Wasielewski, *Coord. Chem. Rev.* **2018**, *361*, 98–119; c) J. Li, P. Li, M. Fan, X. Zheng, J. Guan, M. Yin, *Angew. Chem., Int. Ed.* **2022**, *61*, e202202532; *Angew. Chem.* **2022**, *134*, e202202532; d) M. Mayländer, O. Nolden, M. Franz, S. Chen, L. Bancroft, Y. Qiu, M. R. Wasielewski, P. Gilch, S. Richert, *Chem. Sci.* **2022**, *13*, 6732–6743; e) S.-H. Wang, F. Khurshid, P.-Z. Chen, Y.-R. Lai, C.-W. Cai, P.-W. Chung, M. Hayashi, R.-J. Jeng, S.-P. Rwei, L. Wang, *Chem. Mater.* **2022**, *34*, 4955–4963; f) Y. Xu, J. Zheng, J. O. Lindner, X. Wen, N. Jiang, Z. Hu, L. Liu, F. Würthner, Z. Xie, *Angew. Chem., Int. Ed.* **2020**, *59*, 10363–10367; *Angew. Chem.* **2020**, *132*, 10449–10453.
[84] D. Gosztola, M. P. Niemczyk, W. Svec, A. S. Lukas, M. R. Wasielewski, *J. Phys. Chem. A* **2000**, *104*, 6545–6551.
[85] Y. Li, X. Zhang, D Liu, *J. Photochem. Photobiol. C* **2021**, *48*, 100436.
[86] a) J. Wang, W. Shi, D Liu, Z. Zhang, Y. Zhu, D. Wang, *Appl. Catal. B* **2017**, *202*, 289–297; b) J. Wang, D Liu, Y. Zhu, S. Zhou, S. Guan, *Appl. Catal. B* **2018**, *231*, 251–261.
[87] J. D. Nguyen, E. M. D'Amato, J. M. R. Narayanam, C. R. J. Stephenson, *Nat. Chem.* **2012**, *4*, 854–859.
[88] H. Li, O. S. Wenger, *Angew. Chem., Int. Ed.* **2022**, *61*, e202110491; *Angew. Chem.* **2022**, *134*, e202110491.
[89] N. G. W. Cowper, C. P. Chernowsky, O. P. Williams, Z. K. Wickens, *J. Am. Chem. Soc.* **2020**, *142*, 2093–2099.
[90] E. Doni, B. Mondal, S. O'Sullivan, T. Tuttle, J. A. Murphy, *J. Am. Chem. Soc.* **2013**, *135*, 10934–10937.
[91] a) P. Ruiz-Castillo, S. L. Buchwald, *Chem. Rev.* **2016**, *116*, 12564–12649; b) K. Wang, Z.-H. Deng, S.-J. Xie, D.-D. Zhai, H.-Y. Fang, Z.-J. Shi, *Nat. Commun.* **2021**, *12*, 248.
[92] D. E. C. Corbridge, *Phosphorus: Chemistry, Biochemistry and Technology*, 6th ed., CRC Press, Boca Raton, **2013**.
[93] U. Lennert, P. B. Arockiam, V. Streitferdt, D. J. Scott, C. Rödl, R. M. Gschwind, R. Wolf, *Nat. Catal.* **2019**, *2*, 1101–1106.
[94] P. Blanchard, C. Malacrida, C. Cabanetos, J. Roncali, S. Ludwigs, *Polym. Int.* **2019**, *68*, 589–606.
[95] a) J.-H. Pan, H.-L. Chiu, L. Chen, B.-C. Wang, *Comput. Mater. Sci.* **2006**, *38*, 105–112; b) L. Mayer, L. May, T. J. J. Müller, *Org. Chem. Front.* **2020**, *7*, 1206–1217.
[96] J. P. Barham, M. P. John, J. A. Murphy, *J. Am. Chem. Soc.* **2016**, *138*, 15482–15487.
[97] a) M. H. Aukland, M. Šiaučiulis, A. West, G. J. P. Perry, D. J. Procter, *Nat. Catal.* **2020**, *3*, 163–169; b) K. Sun, A. Shi, Y. Liu, X. Chen, P. Xiang, X. Wang, L. Qu, B. Yu, *Chem. Sci.* **2022**, *13*, 5659–5666.
[98] A. Dewanji, L. van Dalsen, J. A. Rossi-Ashton, E. Gasson, G. E. M. Crisenza, D. Procter, *Nat. Chem.* **2023**, *15*, 43–52.
[99] a) S. O. Poelma, G. L. Burnett, E. H. Discekici, K. M. Mattson, N. J. Treat, Y. Luo, Z. M. Hudson, S. L. Shankel, P. G. Clark, J. W. Kramer, C. J. Hawker, J. Read de Alaniz, *J. Org. Chem.* **2016**, *81*, 7155–7160; b) M. Sneha, A. Bhattacherjee, L. Lewis-Borrell, I. P. Clark, A. J. Orr-Ewing, *J. Phys. Chem. B* **2021**, *125*, 7840–7854; c) E. H. Discekici, N. J. Treat, S. O. Poelma, K. M. Mattson, Z. M. Hudson, Y. Luo, C. J. Hawker, J. Read de Alaniz, *Chem. Commun.* **2015**, *51*, 11705–11708.
[100] K. Nagao, H. Ohmiya, *J. Synth. Org. Chem. Jpn.* **2021**, *79*, 1005–1012.

[101] C. Lampard, J. A. Murphy, N. Lewis, *J. Chem. Soc. Chem. Commun.* **1993**, 295–297.
[102] a) T. Kodo, K. Nagao, H. Ohmiya, *Nat. Commun.* **2022**, *13*, 2684; b) S. Shibutani, T. Kodo, M. Takeda, K. Nagao, N. Tokunaga, Y. Sasaki, H. Ohmiya, *J. Am. Chem. Soc.* **2020**, *142*, 1211–1216; c) S. Shibutani, K. Nagao, H. Ohmiya, *Org. Lett.* **2021**, *23*, 1798–1803; d) M. Nakagawa, K. Nagao, Z. Ikeda, M. Reynolds, I. Ibáñez, J. Wang, N. Tokunaga, Y. Sasaki, H. Ohmiya, *ChemCatChem* **2021**, *13*, 3930–3933.
[103] S. Yakubov, W. J. Stockerl, X. Tian, A. Shahin, M. J. P. Mandigma, R. M. Gschwind, J. P. Barham, *Chem. Sci.* **2022**, *13*, 14041–14051.
[104] N. Kato, T. Nanjo, Y. Takemoto, *ACS Catal.* **2022**, *12*, 7843–7849.
[105] a) J. P. Barham, T. N. J. Fouquet, Y. Norikane, *Org. Biomol. Chem.* **2020**, *18*, 2063–2075; b) C. R. Kennedy, S. Lin, E. N. Jacobsen, *Angew. Chem., Int. Ed.* **2016**, *55*, 12596–12624; *Angew. Chem.* **2016**, *128*, 12784–12814; c) X. Peng, B. M. K. Tong, H. Hirao, S. Chiba, *Angew. Chem., Int. Ed.* **2014**, *53*, 1959–1962; *Angew. Chem.* **2014**, *126*, 1990–1993; d) M. J. P. Mandigma, M. Domański, J. P. Barham, *Org. Biomol. Chem.* **2020**, *18*, 7697–7723.
[106] a) M. C. Fu, R. Shang, B. Zhao, B. Wang, Y. Fu, *Science* **2019**, *363*, 1429–1434; b) J. A. Christensen, B. T. Phelan, S. Chaudhuri, A. Acharya, V. S. Batista, M. R. Wasielewski, *J. Am. Chem. Soc.* **2018**, *140*, 5290–5299.
[107] a) M. Hoshino, H. Uekusa, A. Tomita, S. Koshihara, T. Sato, S. Nozawa, S. Adachi, K. Ohkubo, H. Kotani, S. Fukuzumi, *J. Am. Chem. Soc.* **2012**, *134*, 4569–4572; b) S. Fukuzumi, H. Kotani, K. Ohkubo, *Phys. Chem. Chem. Phys.* **2008**, *10*, 5159–5162.
[108] A. Tlili, S. Lakhdar, *Angew. Chem., Int. Ed.* **2021**, *60*, 19526–19549; *Angew. Chem.* **2021**, *133*, 19678–19701.
[109] B. Zilate, C. Fischer, C. Sparr, *Chem. Commun.* **2020**, *56*, 1767–1775.
[110] a) N. A. Romero, K. A. Margrey, N. E. Tay, D. A. Nicewicz, *Science* **2015**, *349*, 1326–1330; b) D. J. Wilger, J.-M. M. Grandjean, T. R. Lammert, D. A. Nicewicz, *Nat. Chem.* **2014**, *6*, 720–726.
[111] A. Joshi-Pangu, F. Lévesque, H. G. Roth, S. F. Oliver, L.-C. Campeau, D. Nicewicz, D. A. DiRocco, *J. Org. Chem.* **2016**, *81*, 7244–7249.
[112] I. A. MacKenzie, L. Wang, N. P. R. Onuska, O. F. Williams, K. Begam, A. M. Moran, B. D. Dunietz, D. A. Nicewicz, *Nature* **2020**, *580*, 76–80.
[113] a) Y. Zhao, C. Zhang, K. F. Chin, O. Pytela, G. Wei, H. Liu, F. Bureš, Z. Jiang, *RSC Adv.* **2014**, *4*, 30062–30067; b) Z. Hloušková, M. Klikar, O. Pytela, N. Almonasy, A. Růžička, V. Jandová, F. Bureš, *RSC Adv.* **2019**, *9*, 23797–23809.
[114] J. Li, M. Kong, B. Qiao, R. Lee, X. Zhao, Z. Jiang, *Nat. Commun.* **2018**, *9*, 2445.
[115] J. Mateos, F. Rigodanza, A. Vega-Peñaloza, A. Sartorel, M. Natali, T. Bortolato, G. Pelosi, X. Companyó, M. Bonchio, L. Dell'Amico, *Angew. Chem., Int. Ed.* **2020**, *59*, 1302–1312; *Angew. Chem.* **2020**, *132*, 1318–1328.
[116] For selected examples: a) M. Giedyk, R. Narobe, S. Weiß, D. Touraud, W. Kunz, B. König, *Nat. Catal.* **2020**, *3*, 40–47; b) J. Kaur, A. Shahin, J. P. Barham, *Org. Lett.* **2021**, *23*, 2002–2006; c) M. Cybularczyk-Cecotka, J. Predygier, S. Crespi, J. Szczepanik, M. Giedyk, *ACS Catal.* **2022**, *12*, 3543–3549; d) Y.-M. Tian, E. Hofmann, W. Silva, X. Pu, D. Touraud, R. M. Gschwind, W. Kunz, B. König, *Angew. Chem., Int. Ed.* **2023**, *62*, e202218775; *Angew. Chem.* **2023**, *135*, e202218775; for a recent review:; e) L. Brüss, R. Jeyaseelan, J. C. G. Kürschner, M. Utikal, L. Næsborg, *ChemCatChem* **2022**, e202201146.

Manuscript received: December 4, 2022
Revised manuscript received: February 19, 2023
Accepted manuscript online: February 21, 2023
Version of record online: May 9, 2023